

Timothy M. O'Brien

Timing of Iapetus Ocean rifting in the St. Lawrence rift system of southern Quebec, and fault and cleavage dating along the Champlain Thrust of Vermont, Northern Appalachians

Submitted for Publication in:


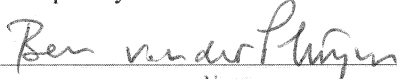
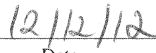


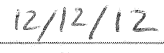

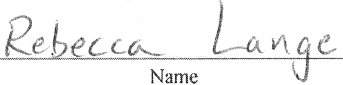
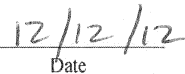
Geology

in lieu of thesis in partial fulfillment of the requirements for the degree of

Master of Science in Geology


Department of Earth and Environmental Sciences

The University of Michigan

 Signature	Accepted by:  Name	 Date
 Signature	 Name	 Date
 Department Chair Signature	 Name	 Date

I hereby grant the University of Michigan, its heirs and assigns, the non-exclusive right to reproduce and distribute single copies of my thesis, in whole or in part, in any format. I represent and warrant to the University of Michigan that the thesis is an original work, does not infringe or violate any rights of others, and that I make these grants as the sole owner of the rights to my thesis. I understand that I will not receive royalties for any reproduction of this thesis.

- Permission granted.
- Permission granted to copy after: _____
- Permission declined.


Author Signature

Earth and Environmental Sciences
 **UNIVERSITY OF MICHIGAN**

Tim O'Brien

Timing of Iapetus Ocean rifting in the St. Lawrence rift
system of southern Quebec, and Fault and cleavage dating
along the Champlain Thrust of Vermont, Northern
Appalachians

MSc. Thesis
University of Michigan
December 2012

Table of Contents

- 1) Timing of Iapetus Ocean rifting from Ar geochronology of pseudotachylytes in the St. Lawrence rift system of southern Quebec.
- 2) Crystallization and resetting of low-temperature muscovite; fault and cleavage dating along the Champlain Thrust (VT), northern Appalachians.
- 3) Data appendix

Tim M. O'Brien

MSc Thesis
University of Michigan
November, 2012

1. Timing of Iapetus Ocean rifting from Ar geochronology of pseudotachylytes in the St. Lawrence rift system of southern Quebec.
2. Crystallization and resetting of low-temperature muscovite; Fault and cleavage dating along the Champlain Thrust (VT), Northern Appalachians.
3. Data appendix.

Timing of Iapetus Ocean rifting from Ar geochronology of pseudotachylytes in the St. Lawrence rift system of southern Quebec

Tim M. O'Brien and Ben A. van der Pluijm

Department of Earth and Environmental Sciences, University of Michigan, 1100 North University Avenue, Ann Arbor, Michigan 48109, USA

ABSTRACT

Laser ablation $^{40}\text{Ar}/^{39}\text{Ar}$ step-heating analyses for encapsulated and unencapsulated pseudotachylytes from a Neoproterozoic normal fault belonging to the St. Lawrence rift system (Canada) preserve the absolute timing of rifting and initial opening of the Iapetus Ocean. The total gas and retention ages for encapsulated pseudotachylytes from the Montmorency fault (Quebec City) are 610.3 ± 4.6 Ma and 619.0 ± 2.5 Ma. Ten unencapsulated analyses from two pseudotachylyte veins with varying matrix/clast ratios yield total gas ages of 634.7 ± 1.6 – 663.9 ± 1.8 Ma. These ages show an excellent linear relationship with the proportion of clast inclusions, resulting in lower intercept ages (i.e., no host rock) of 613.3 and 614.2 Ma. These statistically indistinguishable ages constrain major seismic faulting along the St. Lawrence rift system and significantly improve prior estimates for late Neoproterozoic rifting of Iapetus. The upper intercepts, reflecting host-rock ages, match cooling ages of Grenville basement in the area. We conclude that the time of major continental rifting along the northern Laurentian margin and initiation of the Iapetus Ocean occurred at 613–614 Ma, coeval with emplacement of the 615 Ma Long Range dikes of Labrador. This study also demonstrates that Ar geochronology of pseudotachylytes using varying clast/matrix ratios is a robust method to date ancient faulting.

INTRODUCTION

Since Wilson's (1966) proposal for a proto-Atlantic (Iapetus) Ocean along the eastern margin of Laurentia during the Paleozoic, geologists have variably constrained the timing and history of the creation of this ocean basin in the northern Appalachians (Bond et al., 1984; Williams and Hiscott, 1987; Kamo et al., 1989; Aleinikoff et al., 1995; Cawood et al., 2001). The breakup and end of the Mesoproterozoic supercontinent Rodinia resulted in the formation of two oceans (Pacific and Iapetus) and the formation of Gondwana. Based on paleomagnetic data from the late Precambrian, there are two major competing hypotheses for the formation of Iapetus. Depending on the position of Laurentia (high or low latitude), either Baltica or Amazonia rifted away during the late Neoproterozoic to create an ocean basin. Through the recognition of similar Mesoproterozoic terranes along the eastern margin of Laurentia and Amazonia, it is generally accepted that Amazonia rifted from Laurentia during a series of

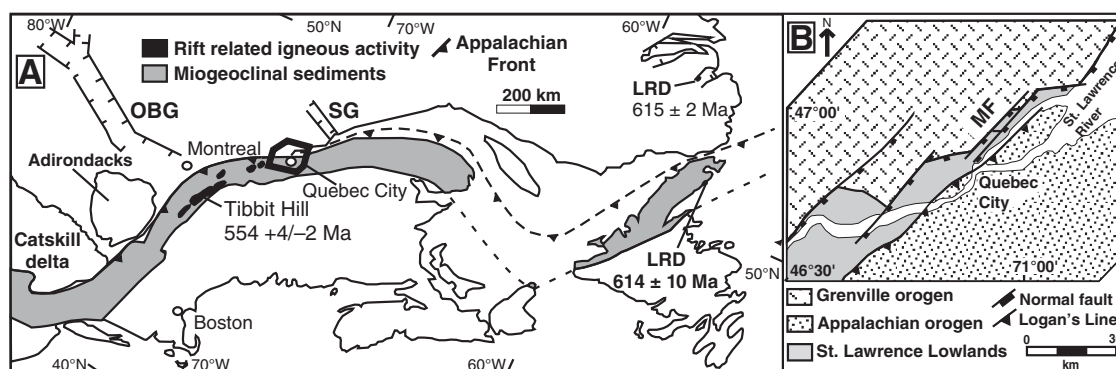
extensional events that are loosely constrained as 620–570 Ma (Keppie et al., 2001; Miller and Barr, 2004). However, due to lack of suitable lithologies and overprinting tectonic events (e.g., the Ordovician Taconic orogeny of the Appalachians) there were no well-constrained radiometric fault ages for late Neoproterozoic rifting between Laurentia and Amazonia; we address this with pseudotachylyte dating in the St. Lawrence rift system.

In the Quebec Appalachians, a system of normal faults containing pseudotachylytes separates ca. 1 Ga Grenville basement rocks from Cambrian–Ordovician sediments of the St. Lawrence Lowlands (Philpotts and Miller, 1963; Tremblay et al., 2003). The area has a long history of faulting, including evidence for frictional melt events preserved in basement rocks (Philpotts and Miller, 1963). Pseudotachylytes are seismically generated melts (e.g., Sibson, 1975) that can be used to determine the time of major faulting. The occurrence of pseudotachylytes indicates dynamic rupture and slip during coseismic displacement (e.g., Swanson, 1992). Radiogenic dating of pseudotachylytes has the potential of accurately determining the age of coseismic brittle faulting, but is hindered by incomplete melting and associated resetting of the host rock (Magloughlin et al., 2001; Warr et al., 2007). This study presents new $^{40}\text{Ar}/^{39}\text{Ar}$ geochronology ages for pseudotachylytes from the Montmorency fault in the northern Appalachians in southern Quebec, using recently developed approaches that overcome most of the past limitations of pseudotachylyte dating, including sample encapsulation and clast/matrix determinations. These new results accurately constrain the late Neoproterozoic (Ediacaran) age of rifting between Laurentia and Amazonia, and thus the initiation of the Iapetus Ocean in this area. Beyond regional implications, this work demonstrates the reliability of multiple subsample dating to determine the absolute ages of melt matrix and incorporated host material in fault rocks.

GEOLOGIC SETTING AND PSEUDOTACHYLYTE DESCRIPTION

Along the eastern margin of Laurentia, U-Pb dating of rhyolites and mafic dikes indicates that Neoproterozoic rifting in the northern Appalachians occurred between 620 and 570 Ma (Kamo et al. 1989; Aleinikoff et al., 1995; Cawood et al., 2001). In the Quebec Appalachians, the St. Lawrence rift system is a set of Neoproterozoic normal faults associated with the opening of the Iapetus Ocean (Fig. 1) (Kumarapeli, 1985). It represents a half-graben structure consisting of listric faults that dip beneath

Figure 1. A: Appalachian orogen in New England and Canada with locations of Appalachian front and Ottawa-Bonnechere (OBG) and Saguenay grabens (SG), failed arms of St. Lawrence rift system (SLRS) (modified from Cawood et al., 2001). Also shown are distributions of miogeoclinal sediments and 615 Ma rift-related Long Range mafic dikes (LRD; Kamo et al., 1989). **B:** Generalized geologic map showing location of normal and transfer faults, including Montmorency fault (MF), of SLRS near Quebec City (modified from Tremblay et al., 2003).



the platform cover sequence and younger Appalachian fold-thrust belt (Tremblay et al., 2003; Allen et al., 2009). The main system of northeast-southwest-trending faults occurs at the contact between Mesoproterozoic rocks of the Grenville basement and Cambrian–Ordovician strata of the St. Lawrence Lowlands. The Ottawa–Bonaventure and Saguenay grabens were characterized as failed rift arms of a rift-rift-rift triple junction that extended into the Grenville basement (Kumarapeli, 1985; Fig. 1A). Fault rocks of the St. Lawrence rift system consist of cataclasites and breccias with several areas containing pseudotachylytes and foliated fault gouge.

Samples were collected from the Montmorency fault, north of Quebec City. The Montmorency fault is a northeast-southwest-trending, steeply dipping normal fault that separates Grenville gneisses to the northwest from Paleozoic sediments to the southeast (Fig. 2A). Surface exposure of the hanging wall of the Montmorency fault reveals a tilted sequence of Ordovician sandstones and shales of the Utica Formation and an interbedded sequence of limestones and shales of the lower Trenton Group in fault contact with Mesoproterozoic gneisses and granitoids of the Laurentides Park Complex. However, drill cores collected from hanging-wall sediments near the Montmorency fault reveal Middle to Late Cambrian passive margin-related Potsdam group sandstones, unconformably overlying Mesoproterozoic basement (Dykstra and Longman, 1995). The deposition

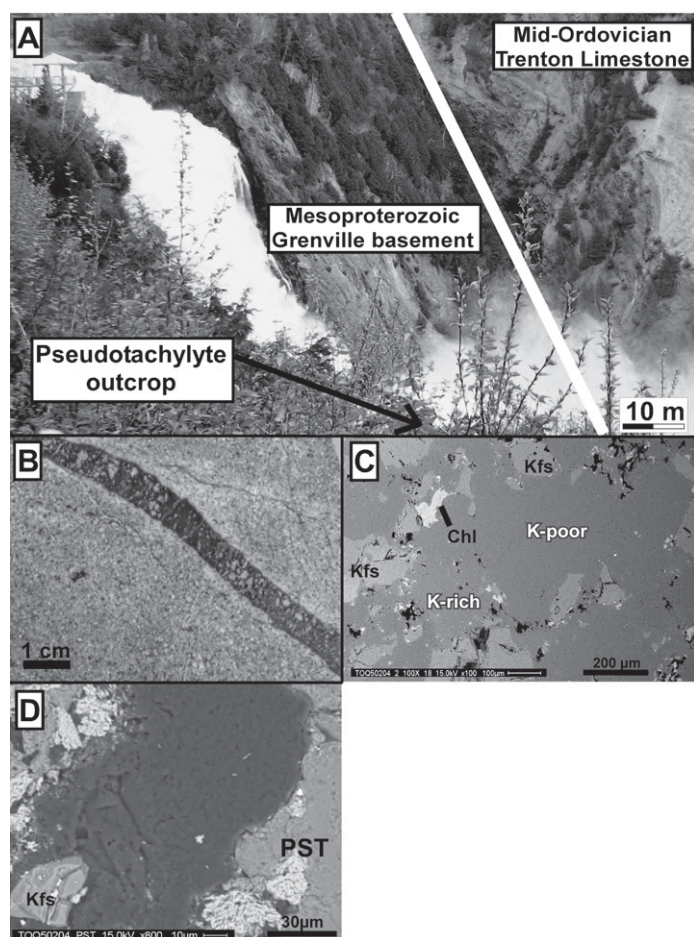


Figure 2. A: Field exposure of steeply dipping Montmorency fault (MF) at Montmorency Falls, north of Quebec City. B: Pseudotachylyte vein found in gneissic host rock of Grenville basement. C: Representative scanning electron microscope image (100 \times magnification) of pseudotachylyte vein displaying potassium-rich and silica-rich matrix and potassium feldspar (Kfs) clasts (Chl—chlorite). D: Silica-rich chilled margin of pseudotachylyte (PST) with potassium feldspar clast.

of these mature quartz-rich sandstones indicates a predominantly shallow subtidal setting (Lewis, 1971), and thickness variations indicate that faults were active during deposition (Dykstra and Longman, 1995). Thus the surface juxtaposition of Ordovician sediments in contact with Precambrian basement reflects early Paleozoic activity along the fault system (Sabourin 1973; Harland and Pickerill, 1982; Tremblay et al., 2003).

In the footwall of the Montmorency fault, Grenville basement contains remarkably well-preserved dark brown and black pseudotachylyte veins (Fig. 2B). These pseudotachylytes typically cut the gneissic foliation of the granitic gneiss wall rock. Matrix compositions reflect the dominant mineralogy of the host rock of quartz + potassium feldspar, and have a heterogeneous distribution of potassium (Fig. 2C). Evidence for friction-induced melting for the formation of these pseudotachylytes is seen in the glassy appearance of the pseudotachylytes and their silica-rich chilled margins on both sides (Figs. 2B and 2D), which are characteristic of rapid quenching from high temperatures (Magloughlin, 1992). Clasts, identified by sharp angular edges, found within the pseudotachylyte matrix include alkali feldspar and quartz with trace amounts of mica and iron oxide. A minor amount of retrograde chlorite is observed around alkali feldspar clasts and feldspar-rich matrix areas.

METHOD

Pseudotachylytes from the Montmorency fault contain an abundance of alkali feldspar and quartz clasts that affect $^{40}\text{Ar}/^{39}\text{Ar}$ dating by producing ages between those of the host rock and melt formation. The incorporation of clasts in pseudotachylyte veins has often given geologically ambiguous ages from $^{40}\text{Ar}/^{39}\text{Ar}$ analyses (e.g., Müller et al., 2002; Di Vincenzo et al., 2004), signifying that clasts are not equilibrated with the matrix or are completely outgassed. To mitigate the effects of clast inclusions, Warr et al. (2007) developed a method that compares the relative abundance (in percent) of clasts within the matrix of a given area in a vein with the age of that sample. Extrapolating the relative abundance of clasts to zero (i.e., all matrix), the age of vein formation is dated; conversely, extrapolating to 100% clasts records the (cooling) age of the host rock. Determining the proportions of clast inclusions was achieved by measuring their total area in a 500X scanning electron microscope (SEM) image. A description of how the relative abundances were determined is provided in the GSA Data Repository¹.

$^{40}\text{Ar}/^{39}\text{Ar}$ Geochronology

In this study, two complementary $^{40}\text{Ar}/^{39}\text{Ar}$ geochronology techniques were used to determine the timing of major displacement on the Montmorency fault: encapsulation dating and multiple subsample dating. Laser ablation $^{40}\text{Ar}/^{39}\text{Ar}$ step-heating analyses were performed on a VG1200S mass spectrometer with 20 s heating times at successively higher powers, following the procedure of Lo Bello et al. (1987).

Quartz Tube Vacuum Encapsulation

One sample was analyzed using a quartz vacuum-encapsulation technique described by Dong et al. (1995) and Magloughlin et al. (2001). With this method, the total gas age represents a minimum age for growth of crystals and the beginning of Ar retention upon cooling; the calculated retention age provides a maximum age for the sample (Magloughlin et al., 2001). By measuring the total gas and retention ages of a pseudotachylyte sample, we are able to bracket the age of melt formation. The major benefit of this technique is the extremely small sample size (<100 μm), which enables the use of small areas that are essentially free of clasts.

¹GSA Data Repository item 2012117, methods, Table DR1, and Figures DR2–DR3, is available online at www.geosociety.org/pubs/ft2012.htm, or on request from editing@geosociety.org or Documents Secretary, GSA, P.O. Box 9140, Boulder, CO 80301, USA.

Multiple Subsamples

In contrast to the small sample size method, subsample analysis allows the inclusion of clasts for dating, but requires that the clast/matrix ratio is determined for at least three samples from a single vein. We analyzed 10 1-mm-sized samples, containing variable amounts of clast inclusions, from 2 pseudotachylyte veins.

RESULTS

Encapsulation Dating

The result for the encapsulated sample by laser step heating yields a total gas age of 610.3 ± 4.6 Ma and a retention age of 619.0 ± 2.5 Ma (Fig. DR1 in the Data Repository), thus constraining vein formation to between 610 and 619 Ma. Based on the criteria provided by McDougall and Harrison (1999), no plateau age can be interpreted from the age spectrum, which has a humped-back geometry. Young ages at low temperatures possibly represent ^{40}Ar loss due to minor chlorite alterations near potassium feldspar clasts and feldspar-rich matrix areas (Fig. DR1).

Subsample Dating

The proportion of clast and matrix was determined for 10 samples from 2 pseudotachylyte veins that exhibit average clast proportions between 9% and 20% (Fig. 3A; Table DR1). The clasts include potassium feldspar and quartz with trace amounts of mica and opaque minerals.

The 10 $^{40}\text{Ar}/^{39}\text{Ar}$ total gas ages for the 2 veins range from 663.53 ± 2.23 Ma for the most clast-rich sample, to 634.98 ± 2.22 Ma for the most clast-poor sample (Figs. DR1 and DR2). All Ar release spectra have similar staircase-shaped degassing patterns (Fig. 3B), which is typical for

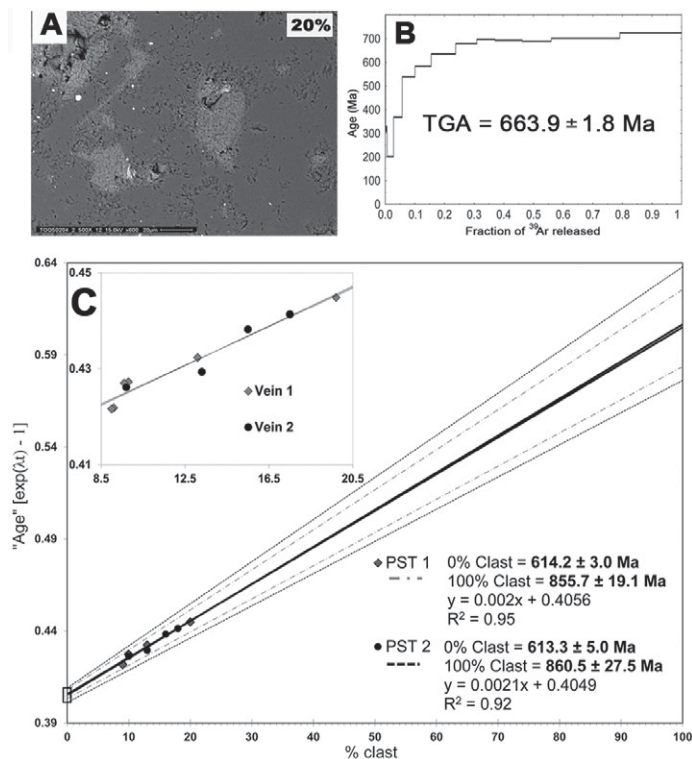


Figure 3. A: Backscattered electron image (500 \times magnification) of unencapsulated sample with 20% clast content. **B:** Degassing spectra for unencapsulated sample with 20% clast content (TGA—total gas age). **C:** Total gas age versus percent clast correlation plot with corresponding regression lines for two pseudotachylyte veins. Inset shows close-up and minimal scatter of data. Plot ages expressed as $\exp(\lambda t - 1)$, where λ is decay constant and t is total gas age.

analyses of mixed phases with varying ages (McDougall and Harrison, 1999). Similar to the encapsulated sample, no plateau age can be interpreted from these spectra, as expected with this approach (Magloughlin et al., 2001). All samples have complex degassing spectra indicative of veins that contain a mixed population with a considerable amount of inherited Ar, which is largely present in potassium feldspar clasts with only a minor amount from incorporated mica clasts.

Figure 3C is a correlation plot between total gas age [represented by $\exp(\lambda t - 1)$, where λ = decay constant and t = total gas age] and proportion of clast for each of the 10 samples from 2 veins. Well-constrained linear regression analyses of six analyses from vein 1 and four analyses from vein 2 intercept the y axis (0% clasts) at 614.2 and 613.3 Ma, respectively; these ages are indistinguishable within error (Fig. 3C). At 100% clasts, the regression lines for veins 1 and 2 intersect at 856 and 861 Ma, respectively (Fig. 3C), reflecting early Neoproterozoic ages that match cooling ages of Grenville host rock in the region (800–900 Ma; e.g., Streepey et al., 2002).

DISCUSSION AND CONCLUSIONS

Pseudotachylyte Ar dating of the Montmorency fault using complementary methods yields ages that significantly refine previous tectonostratigraphic estimates for the timing of late Neoproterozoic continental rifting and Iapetus Ocean formation. Total gas and retention ages determined by vacuum encapsulation and multiple subsample dating provide an age of 613–614 Ma for the timing of fault-related friction melting.

As illustrated in Figure 3C, the timing of major faulting is obtained when the regression lines of multiple analyses intersect the y axis at 0% clasts. Also plotted in Figure 3C, represented by the black box, are the total gas and retention ages for the encapsulated sample of vein 1 that predicts the permissible age range. Ages at the upper end of the regression line, intersecting at 856 and 861 Ma, represent the $^{40}\text{Ar}/^{39}\text{Ar}$ closure ages of host-rock clasts that are typically feldspar rich in these samples. Potassium feldspar closure ages of ca. 850 Ma for the eastern Grenville Province have been reported by several authors (e.g., Cosca et al., 1991; Streepey et al., 2002), matching our results.

The ages obtained for the Montmorency fault significantly constrain the geological evidence for Ediacaran rifting and the breakup of Rodinia in the northern Appalachians (van Staal et al., 1998; Cawood et al., 2001). The results presented in this study match paleomagnetic reconstructions that require a pre-570 Ma opening of the Iapetus Ocean. The presence of pseudotachylytes demonstrates that the Montmorency fault was active during extensional faulting along the Laurentian margin in the late Neoproterozoic at 613–614 Ma, coeval with the 615 Ma Long Range dikes of Labrador (Kamo et al., 1989). Based on paleomagnetic and sedimentologic data, continental breakup may have continued until ca. 570 Ma, when Iapetus seafloor spreading commenced (Williams and Hiscott, 1987; Cawood et al., 2001; Cawood and Nemchin, 2001). In Newfoundland, stratigraphic evidence for the timing of rifting began with the deposition of late Neoproterozoic–early Cambrian Bradore Formation sandstone and conglomerate. Continued subsidence of an evolving passive margin places the rift-drift transition at the Precambrian–Cambrian boundary (Williams and Hiscott, 1987; Allen et al., 2009). The presence of an ocean basin outboard of the Iapetan margin by the late Ediacaran is also recorded in zircons from ocean island basalt seamount magmatism of the Tibbit Hill volcanics (554 Ma; Kumarapeli et al., 1989) in southern Quebec and the Skinner Cove volcanics (550 Ma; Cawood et al., 2001) in Newfoundland. Thus we interpret our pseudotachylyte ages as the initiation of rift faulting that led to the formation of Laurentia's Iapetus margin.

The $^{40}\text{Ar}/^{39}\text{Ar}$ pseudotachylyte age from this study combined with K-Ar analyses of brittle fault gouge and apatite fission-track analyses of Tremblay et al. (2007) illustrate a long, >400 m.y. deformation history along the Montmorency fault. The early phase of deformation, as presented in this study, took place at 613–614 Ma (Ediacaran), when coseismic

normal faulting and extension occurred as the result of continental rifting over a hypothesized mantle plume (Burke and Dewey, 1973; Kumarapeli, 1985). Later deformation along the fault system occurred between 465 and 445 Ma and during Mesozoic exhumation (Tremblay et al., 2007; Tremblay and Roden-Tice, 2010), interpreted as normal fault reactivation from tectonic loading (Jacobi, 1981) and far-field tectonic activity from North Atlantic rifting. The fine-grained microstructure of pseudotachylyte veins and relatively low metamorphic grade in the region resisted resetting of the isotopic system, preserving the old ages. Beyond the regional implications, our study also illustrates a robust approach to pseudotachylyte dating that overcomes the limitations of previous efforts that were hampered by representative sample sizes and host-rock inclusions.

ACKNOWLEDGMENTS

Research was supported by National Science Foundation grant EAR-0738435 to van der Pluijm and a University of Michigan Turner Research Grant to O'Brien. We are grateful for the help of Chris Hall at the University of Michigan argon laboratory. We thank Phil McCausland, Joe Meert, and an anonymous reviewer for constructive comments that improved the presentation of regional implications.

REFERENCES CITED

- Aleinikoff, J.N., Zartman, R.E., Walter, M., Rankin, D.W., Lyttle, P.T., and Burton, W.C., 1995, U-Pb ages of metarhyolites of the Catoctin and Mount Rogers formations, central and southern Appalachians: Evidence for two phases of Iapetan rifting: *American Journal of Science*, v. 295, p. 428–454, doi:10.2475/ajs.295.4.428.
- Allen, J.S., Thomas, W.A., and Lavoie, D., 2009, Stratigraphy and structure of the Laurentian rifted margin in the northern Appalachians: A low-angle detachment rift system: *Geology*, v. 37, p. 335–338, doi:10.1130/G25371A.1.
- Bond, G.C., Nickeson, P.A., and Kominz, M.A., 1984, Breakup of a supercontinent between 625 Ma and 555 Ma: New evidence and implications for continental histories: *Earth and Planetary Science Letters*, v. 70, p. 325–345, doi:10.1016/0012-821X(84)90017-7.
- Burke, K., and Dewey, J., 1973, Plume-generated triple junction, key indicators in applying plate tectonics to old rocks: *Journal of Geology*, v. 81, p. 406–433, doi:10.1086/627882.
- Cawood, P.A., and Nemchin, A.A., 2001, Paleogeographic development of the east Laurentian margin: Constraints from U-Pb dating of detrital zircons in the Newfoundland Appalachians: *Geological Society of America Bulletin*, v. 113, p. 1234–1246, doi:10.1130/0016-7606(2001)113<1234:PDOTEL>2.0.CO;2.
- Cawood, P.A., McCausland, P.J.A., and Dunning, G.R., 2001, Opening Iapetus: Constraints from the Laurentian margin in Newfoundland: *Geological Society of America Bulletin*, v. 113, p. 443–453, doi:10.1130/0016-7606(2001)113<0443:OICFTL>2.0.CO;2.
- Cosca, M.A., Sutter, J.F., and Essene, E.J., 1991, Cooling and inferred uplift/erosion history of the Grenville orogen, Ontario: Constraints from $^{40}\text{Ar}/^{39}\text{Ar}$ thermochronology: *Tectonics*, v. 10, p. 959–977, doi:10.1029/91TC00859.
- Di Vincenzo, G., Rocchi, S., Rossetti, F., and Storti, F., 2004, $^{40}\text{Ar}/^{39}\text{Ar}$ dating of pseudotachylytes: The effect of clast-hosted extraneous argon in Cenozoic fault-generated friction melts from the West Antarctic rift system: *Earth and Planetary Science Letters*, v. 223, p. 349–364, doi:10.1016/j.epsl.2004.04.042.
- Dong, H., Hall, C.M., Peacor, D.R., and Halliday, A.N., 1995, Mechanisms of argon retention in clays revealed by later $^{40}\text{Ar}/^{39}\text{Ar}$ dating: *Science*, v. 267, p. 355–359, doi:10.1126/science.267.5196.355.
- Dykstra, J.C.F., and Longman, M.W., 1995, Gas reservoir potential of the lower Ordovician Beekmantown group, Quebec Lowlands, Canada: *American Association of Petroleum Geologists Bulletin*, v. 79, p. 513–530.
- Harland, T.L., and Pickerill, T.L., 1982, A review of Middle Ordovician sedimentation in the St. Lawrence Lowland, eastern Canada: *Geological Journal*, v. 17, p. 135–156, doi:10.1002/gj.3350170205.
- Jacobi, R.D., 1981, Peripheral bulge—A causal mechanism for the Lower/Middle Ordovician unconformity along the western margin of the Northern Appalachians: *Earth and Planetary Science Letters*, v. 56, p. 245–251, doi:10.1016/0012-821X(81)90131-X.
- Kamo, S.L., Gower, C.F., and Kroch, T.E., 1989, Birthdate for the Iapetus ocean? A precise U-Pb zircon and baddeleyite age for the Long Range dikes, south-east Labrador: *Geology*, v. 17, p. 602–605, doi:10.1130/0091-7613(1989)017<0602:BFTLOA>2.3.CO;2.
- Keppie, J.D., Dostal, J., Ortega-Gutiérrez, F., and Lopez, R., 2001, A Grenvillian arc on the margin of Amazonia: Evidence from the southern Oaxacan Complex, southern Mexico: *Precambrian Research*, v. 112, p. 165–181, doi:10.1016/S0301-9268(00)00150-9.
- Kumarapeli, P.S., 1985, Vestiges of Iapetan rifting in the craton of the Northern Appalachians: *Geoscience Canada*, v. 12, p. 54–59.
- Kumarapeli, P.S., Dunning, G.R., Pintson, H., and Shaver, J., 1989, Geochemistry and U-Pb zircon age of comenditic metafelsites of the Tibbit Hill Formation, Quebec Appalachians: *Canadian Journal of Earth Sciences*, v. 26, p. 1374–1383, doi:10.1139/e89-117.
- Lo Bello, P., Fraud, G., Hall, C.M., York, D., Lavina, P., and Bernat, M., 1987, $^{40}\text{Ar}/^{39}\text{Ar}$ step-heating and laser fusion dating of a Quaternary volcano from Neschers, Massif Central, France: The defeat of xenocrystic contamination: *Chemical Geology*, v. 66, p. 61–71, doi:10.1016/0168-9622(87)90029-7.
- Magloughlin, J.F., 1992, Microstructural and chemical changes associated with cataclasis and friction melting at shallow crustal levels: The cataclasis-pseudotachylyte connection: *Tectonophysics*, v. 204, p. 243–260, doi:10.1016/0040-1951(92)90310-3.
- Magloughlin, J.F., Hall, C.M., and van der Pluijm, B.A., 2001, $^{40}\text{Ar}/^{39}\text{Ar}$ geochronology of pseudotachylytes by vacuum encapsulation: North Cascade Mountains, Washington, USA: *Geology*, v. 29, p. 51–54, doi:10.1130/0091-7613(2001)029<0051:AAGOPB>2.0.CO;2.
- McDougall, I., and Harrison, T.M., 1999, *Geochronology and thermochronology by the $^{40}\text{Ar}/^{39}\text{Ar}$ method* (second edition): Oxford, UK, Oxford University Press, 212 p.
- Miller, B.V., and Barr, S.M., 2004, Metamorphosed gabbroic dikes related to opening of Iapetus ocean at the St. Lawrence Promontory: Blair River Inlier, Nova Scotia, Canada: *Journal of Geology*, v. 112, p. 277–288, doi:10.1086/382759.
- Müller, W., Kelly, S.P., and Villa, I.M., 2002, Dating fault-generated pseudotachylytes: Comparison of $^{40}\text{Ar}/^{39}\text{Ar}$ stepwise-heating, laser-ablation and Rb-Sr microsampling analyses: *Contributions to Mineralogy and Petrology*, v. 144, p. 57–77, doi:10.1007/s00410-002-0381-6.
- Philpotts, A.R., and Miller, J.A., 1963, A Pre-Cambrian glass from St. Alexis-des-Monts, Quebec: *Geological Magazine*, v. 100, p. 337–343, doi:10.1017/S0016756800056077.
- Sabourin, R., 1973, *Geology of part of the Beaupré Seigneury: Department of Natural Resources of Québec Preliminary Report 600*, 19 p.
- Sibson, R.H., 1975, Generation of pseudotachylytes by ancient seismic faulting: *Royal Astronomical Society Geophysical Journal*, v. 43, p. 775–794, doi:10.1111/j.1365-246X.1975.tb06195.x.
- Streepey, M.M., Hall, C.M., and van der Pluijm, B.A., 2002, The $^{40}\text{Ar}/^{39}\text{Ar}$ laser analysis of K-feldspar: Constraints on the uplift history of the Grenville Province in Ontario and New York: *Journal of Geophysical Research*, v. 107, 2296, doi:10.1029/2001JB001094.
- Swanson, M.T., 1992, Fault structure, wear mechanisms and rupture processes in pseudotachylyte generation: *Tectonophysics*, v. 204, p. 223–242, doi:10.1016/0040-1951(92)90309-T.
- Tremblay, A., Long, B., and Massé, M., 2003, Supracrustal faults of the St. Lawrence rift system, Québec: Kinematics and geometry as revealed by field mapping and marine seismic reflection data: *Tectonophysics*, v. 369, p. 231–252, doi:10.1016/S0040-1951(03)00227-0.
- Tremblay, A., Sasseville, C., Clauer, N., and Zentilli, M., 2007, The St. Lawrence Rift System in eastern Canada—Field and isotopic evidence for Paleozoic to Mesozoic(?) reactivations of Iapetus faults: *Geological Society of America Abstracts with Programs*, v. 39, no. 1, p. 95.
- Tremblay, A., and Roden-Tice, M.K., 2010, Iapetan versus Atlantic rifting of Laurentia—Constraints from field mapping and AFT dating of Precambrian basement rocks, Canada: *Geological Society of America Abstracts with Programs*, v. 42, no. 1, p. 79.
- van Staal, C.R., Dewey, J.F., Mac Niocaill, C., and McKerrow, W.S., 1998, The Cambrian-Silurian tectonic evolution of the northern Appalachians and British Caledonides: History of a complex, west and southwest Pacific-type segment of Iapetus, in Blundell, D.J., and Scott, A.C., eds., *Lyell: The past is the key to the present: Geological Society of London Special Publication 143*, p. 199–242, doi:10.1144/GSL.SP.1998.143.01.17.
- Warr, L.N., van der Pluijm, B.A., and Tourscher, S., 2007, The age and depth of exhumed friction melts along the Alpine fault, New Zealand: *Geology*, v. 35, p. 603–606, doi:10.1130/G23541A.1.
- Williams, H., and Hiscott, R.N., 1987, Definition of the Iapetus rift-drift transition in western Newfoundland: *Geology*, v. 15, p. 1044–1047, doi:10.1130/0091-7613(1987)15<1044:DOTLRT>2.0.CO;2.
- Wilson, J.T., 1966, Did the Atlantic close and then re-open?: *Nature*, v. 211, p. 676–681, doi:10.1038/211676a0.

Manuscript received 27 July 2011

Revised manuscript received 19 December 2011

Manuscript accepted 26 December 2011

Printed in USA

1 Crystallization and resetting of low-temperature muscovite; Fault and cleavage
2 dating along the Champlain Thrust (VT), Northern Appalachians

3 **Tim M. O'Brien**

4 **Chris M. Hall**

5 **Ben A. van der Pluijm**

6

7 **Abstract**

8 $^{40}\text{Ar}/^{39}\text{Ar}$ step-heating analyses were performed on fine-grained muscovite separates
9 from low-grade (anchizonal) mylonites and slates to test a new approach in interpreting
10 $^{40}\text{Ar}/^{39}\text{Ar}$ results for fine-grained clays in fault gouge. The Champlain fault in northwestern
11 Vermont is an ideal site to study $^{40}\text{Ar}/^{39}\text{Ar}$ geochronology and thermochronology of fine-grained
12 illite in phyllonites and slates. Being among the first descriptions of a thrust fault, the temporal
13 history and geochronologic age of the Champlain thrust has never been determined remained
14 enigmatic. We present an illite characterization and $^{40}\text{Ar}/^{39}\text{Ar}$ step-heating study of phyllonites
15 from the Champlain thrust and slates from the footwall Ordovician Iberville Formation. Laser-
16 ablation $^{40}\text{Ar}/^{39}\text{Ar}$ step-heating analyses were conducted on two samples from a 2-3 m thick
17 phyllonite (center and contact with hanging wall) and a thinly cleaved slate containing micron to
18 submicron illite grains. Illite crystallinity and microstructural observations show that the
19 phyllonites and slates experienced anchizonal metamorphism (~200-300 °C). X-ray polytype
20 quantification and TEM imaging show that the samples contain a mixture of detrital and
21 authigenic $2M_1$ and diagenetic $1M_d$ illite. Sample collected at the center of the phyllonite,
22 $^{40}\text{Ar}/^{39}\text{Ar}$ analyses of the two finer grain-size fractions yield retention ages of 338 Ma, while a

23 third coarser fraction produces a retention age of 376 Ma. For the hanging-wall contact sample,
24 all three grain-size fractions yield $^{40}\text{Ar}/^{39}\text{Ar}$ retention ages around 260 Ma. Linear mixing
25 modeling of total gas and retention $^{40}\text{Ar}/^{39}\text{Ar}$ ages from illite separates from the Iberville
26 Formation yielded an age of 350.6 ± 1.2 Ma for the timing of slaty cleavage formation. These
27 results suggest that, following initial Middle to Late Ordovician emplacement, the Champlain
28 thrust experienced two pulses of late Paleozoic metamorphism and deformation. Silurian – E.
29 Mississippian, Acadian-Neoacadian tectonism caused clay mineral transformations and isotopic
30 loss of ^{40}Ar by diffusion in illite in the Champlain Thrust and Iberville Formation. The second
31 pulse caused thermal resetting and overprinting of Acadian-Neoacadian illite that is localized
32 along the boundary with the hanging wall during the L. Mississippian – Permian Alleghanian
33 Orogeny. Regionally, our results show that thermal effects associated with the Acadian-
34 Neoacadian and Alleghanian orogenies caused low-grade clay transformations as far away as
35 northwestern Vermont.

36

37 **Introduction**

38 To understand the deformation history of low-grade (subgreenschist facies) orogenic
39 terranes, $^{40}\text{Ar}/^{39}\text{Ar}$ geochronology of micron-to-submicron illite/muscovite grains presents a
40 potentially powerful approach for estimating the timing of low-grade metamorphism, cleavage
41 formation, hydrothermal alteration, and shallow-to-mid crustal faulting (Hunziker et al., 1986;
42 Reuter and Dallmeyer, 1987; Kirschner et al. 1996; Dong et al., 1997; Hall et al., 1997, 2000;
43 van der Pluijm et al., 2001, 2006). Due to the small sizes of illite grains, single-crystal dating
44 cannot be used and instead analyses are done using grain-size fractions that contain many

45 individual sub-micron sized grains. Many studies have reported geologically complicated ages,
46 which have been interpreted as the result of (1) mixed populations of neo-formed grains and
47 detrital grains (Hower et al., 1963; Hurley et al., 1963; West and Lux, 1993; Kirschner et al.
48 1996; Dunlap, 1997) that differ in crystallization age and Ar retention; (2) incomplete resetting
49 of the argon system due to the low temperatures at which they experienced deformation
50 (Hunziker et al., 1986; Reuter and Dallmeyer, 1987; Dunlop, 1997); (3) ^{40}Ar diffusional loss by
51 intracrystalline deformation (Kligfield et al. 1986; Mulch et al. 2002; Cosca et al. 2011); and (4)
52 ^{39}Ar loss by recoil during irradiation, resulting in ages that are older than stratigraphic ages
53 (Turner and Cadogan, 1974, Foland et al., 1984, Dong et al., 1995).

54 In this study we present $^{40}\text{Ar}/^{39}\text{Ar}$ laser degassing and vacuum encapsulation step-heating
55 experiments of fine-grained ($\leq 2\ \mu\text{m}$) white mica from phyllonites of the Champlain Thrust and
56 footwall slates, located in the foreland fold-thrust belt of the northern Appalachians (Fig. 1).
57 Vacuum encapsulation allows for the measurement of ^{39}Ar that is lost through recoil and
58 measurement of ^{40}Ar and ^{39}Ar that remains in the clay during irradiation. Combining all ^{39}Ar
59 with radiogenic ^{40}Ar yields a total gas age, which is functionally equivalent to a conventional K-
60 Ar age (Dong et al. 1995). The total gas age model assumes there is no K in non-retentive sites
61 and therefore all ^{39}Ar lost during neutron irradiation should be attributed to K in sites that have
62 retained ^{40}Ar (Dong et al., 1995; Hall et al., 2000 and refs therein). By contrast, an “argon
63 retention age” may be calculated solely from Ar isotopes retained within the clay sample during
64 irradiation. The retention age model assumes that ^{39}Ar is lost during irradiation from the same
65 sites that lost ^{40}Ar in nature (Dong et al. 1995; 1997). In essence, it assumes that K resides in
66 non-retentive sites and those sites have contributed to the total ^{39}Ar inventory, but have not
67 produced retained radiogenic ^{40}Ar .

68 The total gas age model and the retention age model are two end-member interpretations.
69 The total gas age model assumes that there is no K in defect sites that are responsible for loss of
70 ³⁹Ar due to recoil while the retention age model assumes that K concentrations within defect
71 sites are the same as for sites that can retain Ar isotopes. Several studies have been performed in
72 an attempt to determine the appropriate conditions in which to apply one model over the other
73 (Dong et al., 1997, 2000; Hall et al., 1997; Hnat, 2009). These studies have focused on applying
74 the models to accurately date the timing of deposition of units in sedimentary basins (e.g., Gulf
75 Coast, Welsh Basin, and Appalachian Basin) or hydrothermal mineral deposits (i.e. Twin Creeks
76 deposit, Nevada) (Dong et al., 1997, 2000; Hall et al. 1997, 2000). The main criteria with which
77 one model was selected over the other included grain-size, degree of diagenesis or low-grade
78 metamorphism, and the proportion of smectite.

79 Even though the Champlain fault was one of the first accurate descriptions of a thrust
80 fault ever published (Emmons, 1842), the precise age of its development remains unknown.
81 Results from this study are used to determine: (1) the appropriate ⁴⁰Ar/³⁹Ar age model for dating
82 of subgreenschist fine-grained white mica in the Champlain Thrust and similar faults; (2) the
83 mechanism for timing of deformation (i.e. thermal overprinting, intracrystalline deformation, or
84 neocrystallization); (3) the timing of the formation of the Champlain thrust; (4) the timing of
85 metamorphism and cleavage formation in western Vermont. To determine the appropriate
86 ⁴⁰Ar/³⁹Ar age model and deformation mechanism, illite crystallinity measurements and X-ray
87 polytype quantification were performed to establish the size and degree of crystallinity of illites
88 packets of the Champlain Thrust and Iberville Formation samples. Transmission Electron
89 Microscopy (TEM) images were collected to optically confirm illite crystallinity and polytype
90 results.

91

92 **Geologic Setting and Fault Description**

93 *Geologic Setting*

94 Geochronology and fossil evidence support the interpretation of three major Paleozoic
95 orogenic events that formed the present day New England Appalachians. The first of these three
96 events is referred to as the Mid-to-Late Ordovician Taconic orogeny. This event occurred as the
97 result of the collision of a volcanic arc (Tucker and Robinson, 1990) or arcs (Karabinos et al.,
98 1998) with the eastern edge of Laurentia, beginning around 470 Ma and continuing through
99 approximately 445 Ma (Tucker and Robinson, 1990; Ratcliff et al., 1998; van Staal, 2007).
100 Taconic deformation in the northern Appalachian foreland fold-thrust belt consists of westward
101 propagating allochthonous and parautochthonous thrust sheets composed of slope/rise and
102 carbonate shelf sediments onto the Laurentian continental platform (Fig. 1; Bird and Dewey,
103 1970; Zen, 1972; Stanley and Ratcliffe, 1985). Continued convergence led to the Late Silurian –
104 Carboniferous Acadian-Neocadian orogeny that resulted from the collision between Laurentia
105 and the composite Avalon terrane (Bird and Dewey, 1970; Robinson et al., 1998; van Staal,
106 2007). Effects of the Acadian-Neocadian orogeny include Silurian-Devonian plutonism, large
107 recumbent folding and faulting, and regional metamorphism (greenschist to granulite facies)
108 (Robinson et al., 1998). The final orogenic event in the northern Appalachians, the Alleghanian
109 orogeny, occurred during the Late Mississippian to the Permian (Rankin, 1994; Wintsch et al.,
110 2003; Hatcher, 2010). The Alleghanian orogeny is attributed to the final, oblique collision of
111 Laurentia and Gondwana in the formation of the supercontinent Pangaea (Hatcher, 2002, 2010).
112 Deformation attributed to the Alleghanian orogeny includes dextral strike-slip faulting and

113 metamorphism, which overprint earlier Taconic and Acadian-Neoacadian structures (Mosher,
114 1983; Moecher, 1999).

115 In the parautochthonous foreland, the Champlain Thrust stretches from northern Vermont
116 (near the international border, where it becomes the Logan's Line of southern Quebec) down to
117 New York where it known as the Taconic Frontal Thrust (Rowley and Kidd,1981) (Fig. 1). In
118 northern Vermont, the Champlain Thrust separates parautochthonous Cambrian through
119 Ordovician shelf sequence sedimentary rocks from autochthonous shelf sequence sedimentary
120 rocks (Fig 1). To the south, near Albany NY (Fig. 1), the fault separates allochthonous slope and
121 rise siliclastic strata of the Taconic allochthon and Ordovician flysch sediments from Cambrian
122 through Ordovician shelf sequence sedimentary strata and Ordovician flysch (Rowley et al.,
123 1981, Rowley, 1983, Stanley and Ratcliff, 1985). Using trigonometric relationships, Rowley and
124 Kidd (1982) suggest that there is >80 km of westward displacement along the thrust fault. As
125 stated above, the age of the Champlain Thrust is not well-constrained and there have been
126 numerous theories put forth claiming to have determined the age of the movement. Welby (1961)
127 was one of the first to claim that the Champlain Thrust developed during the Mid to Late
128 Ordovician Taconic Orogeny, while Cady (1969) proposed that it developed during the
129 Devonian Acadian Orogeny. The latter idea was short lived, since the youngest stratigraphic unit
130 that is cut by the fault is Middle Ordovician. The Mid to Late Ordovician age was later
131 reconfirmed by Rowley and Kidd (1981) and Stanley and Ratcliff (1985) and is the age generally
132 accepted today.

133 North of Burlington, at Lone Rock Point, (study area, Fig. 2) the Champlain Thrust
134 strikes north-south and dips shallowly to the east (<20°) and is interpreted to root in within the
135 Middle Proterozoic Green Mountain Massif (Stanley and Ratcliff, 1985). The fault places lower

136 Cambrian Dunham Dolomite over deformed Middle Ordovician Iberville Formation flysch
137 sedimentary rocks (Fig. 2).

138 ***Fault Rock Description***

139 At Lone Rock Point, fault rocks associated with the Champlain Thrust fault are
140 approximately 2-3 meters thick and consist of black fault gouge and 1-mm to 5-cm thick
141 carbonate veins (Fig. 3A and B). X-ray diffraction of bulk-rock samples shows that the clay-rich
142 layers consist predominantly of illite/muscovite, calcite, quartz, with minor amounts of dolomite,
143 plagioclase and K-feldspar. In the center of the fault, calcite layers show ductile deformation
144 through asymmetric isoclinal folding with a westward vergence direction and boudinaged
145 carbonate veins parallel to the mylonitic foliation (Fig. 3C). Near the contact of the fault with
146 the hanging wall, the Champlain Thrust displays highly deformed fault rock and the contact with
147 the comparatively undeformed overlying Dunham dolomite is very sharp with only minor
148 fracturing in the dolomite. Structures of the fault gouge at the boundary with the hanging wall
149 include C-C' (Fig. 3D) and S-C fabrics with a westward transport direction.

150 The Champlain Thrust contains carbonate porphyroclasts which consist predominantly of
151 calcite with minor amounts of quartz (Fig. 4A). In the porphyroclasts, calcite exhibits ductile
152 behavior (Fig. 4B) while quartz remains dominantly brittle (Fig. 4C). Calcite grains in the clasts
153 are highly twinned but are partially dissolved at the grain boundaries, ending before the
154 boundary is reached (Fig. 4B). Large quartz grains found within the porphyroclasts exhibit
155 fracturing and intracrystalline deformation, characterized by undulose extinction and sub-grain
156 formation (Fig. 4C). The combination of plastic deformation in calcite and brittle-ductile
157 deformation of quartz indicates deformation temperatures <300°C, probably between 200-300°C.

158

159 *Iberville Formation*

160 The Iberville Formation is a noncalcareous shale that is rhythmically interbedded with
161 thin dolomite layers (Hawley, 1957). At Mt. Philo, in northwestern Vermont, the Iberville Fm. is
162 a thinly cleaved argillaceous slate with minor calcareous interlayers (Fig. 3E). The cleavage
163 strikes roughly N-S, parallel to the strike of the Champlain Thrust. XRD analyses of bulk
164 samples indicate that the Iberverille Fm. slates are made up of illite/muscovite, chlorite, calcite,
165 quartz and minor amounts of dolomite, plagioclase and K-feldspar.

166

167 **METHODS**

168 *Fault Dating*

169 It has been shown that during neutron irradiation, the energy released during production
170 of ³⁹Ar corresponds to a recoil distance of ~160 Å (Turner and Codogan, 1974; Foland et al.,
171 1984; Dong et al., 1995, 1997). Illite grains typically have thicknesses less than or roughly equal
172 to this distance, so irradiation can cause ³⁹Ar to be lost via low-retention sites in illite separates
173 (Dong et al., 1995). To account for ³⁹Ar loss from fine-grained samples, illite separates were
174 vacuum encapsulated in quartz tubes before irradiation. Step-heating experiments of vacuum
175 encapsulated irradiated illite separates showed that the proportion of ³⁹Ar released before step-
176 heating begins (the amount released from the tube after it is broken open at room temperature) is
177 inversely correlated with illite crystallinity. This implies that thick, well-crystallized illite
178 packets are more Ar retentive (both for ³⁹Ar produced during irradiation and ⁴⁰Ar produced in

179 nature) than thin, poorly crystallized illite packets in nature (Dong et al., 1995; Hall et al., 2000
180 and refs therein).

181 During vacuum encapsulation step-heating experiments, the inclusion of the ^{39}Ar lost to
182 recoil measured at room temperature corresponds to the total gas age. Omitting the ^{39}Ar lost to
183 recoil provides the retention age. The total gas age model assumes that there is no ^{40}Ar lost in
184 nature (Dong et al., 1995), while the retention age model assumes that ^{39}Ar is lost during
185 irradiation for the same sites that lost ^{40}Ar in nature (Dong et al., 1997; Hall et al., 2000). It has
186 been shown (Hnat, 2009) that the retention age model is appropriate for illite samples with large,
187 well-crystallized, packet thicknesses and containing little or no smectite. Conversely, the total
188 gas age model is appropriate for samples where K is leached from all potential low-retention
189 sites, so that there is no ^{39}Ar production from low-retention sites. There is a correlation between
190 the average packet thickness and the amount of ^{39}Ar lost to recoil as well as amount of
191 expandable interlayers in I/S crystallites creating imperfections that act as pathways for
192 radiogenic ^{40}Ar diffusion loss in nature or ^{39}Ar loss in the reactor (Dong et al., 1995; 2000; Hall
193 et al., 1997, 2000).

194 **Sample preparation:** Samples collected from the Champlain thrust and the Iberville Fm.
195 slates at Mt. Philo were centrifuged into three grain-size fractions (<0.05, 0.05 – 0.2, and 0.2 – 2
196 μm). By applying Stokes Law to the centrifuge process, the three grain-size fractions can be
197 separated. Prior to irradiation, illite samples were placed in fused silica vials for vacuum-
198 encapsulation to measure ^{39}Ar recoil loss. The irradiation standard used was hornblende standard
199 MMhb-1 with a K-Ar age of 520.4 Ma (Samson and Alexander, 1987). $^{40}\text{Ar}/^{39}\text{Ar}$ step heating
200 were performed on the VG1200S noble gas mass spectrometer using a continuous laser fusion
201 system at the University of Michigan.

202

203 *Illite Crystallinity*

204 Illite crystallinity (IC) is a XRD based technique that determines the grade of low-grade
205 metapelites (Kisch, 1983; Frey, 1987; Merriman and Peacor, 1999; Kübler and Jaboyedoff,
206 2000). Illite is a non-expanding, potassium-deficient phyllosilicate that has a composition near
207 muscovite. It is made up of crystallites or ‘packets’ of 1-nm thick sheets of 2:1 structured
208 tetrahedral and octahedral aluminosilicate layers bonded to other grains by interlayered
209 potassium cations (Moore and Reynolds, 1997; Meunier and Velde, 2004). The IC technique
210 measures the change in the in shape of the basal reflection of 1-nm illite XRD peak at one-half of
211 its height above the background. The measurement is typically expressed as the change in the
212 Bragg angle, $\Delta^{\circ}2\theta$, where $^{\circ}2\theta$ is the XRD angle (Kübler, 1967; Kirsh, 1980; Kübler and
213 Jaboyedoff, 2000). As the thickness of the packets increases the width of the 1-nm XRD peak
214 narrows, which in turn decreases the IC. This indicates that there is an inverse relationship
215 between packet size and peak width. IC is also influenced by the presence of expandable
216 interlayers (i.e. smectite). Expandable interlayers, such as smectite, will broaden the 1-nm XRD
217 peak leading to higher IC values (Eberl and Velde, 1989; Jaboyedoff, 2001).

218 IC values are typically used to define subgreenschist facies metapelitic zones: IC values
219 $>0.42^{\circ}2\theta$ correspond to the diagenetic zone (zeolite facies). IC values between 0.25 and 0.42 lie
220 within the anchizonal (prehnite-pumpellyite facies), while IC values <0.25 correspond to the
221 epizone (greenschist facies).

222 **Sample preparation:** IC values can be affected by several sample preparation factors
223 including: slurry thickness, machine variations and grain-size (e.g. Kisch and Frey, 1987; Kisch,

224 1991; Warr and Rice, 1994). Modifying the methodology of Verdel et al. (2011), approximately
225 8 mg of a $\leq 2\mu\text{m}$ clay-water mixture was pipetted on a glass slide and left to dry overnight. The \leq
226 $2\mu\text{m}$ size fraction is recommended for IC measurements since this fraction contains the most
227 crystallites that contribute to the $1\mu\text{m}$ peak profile (Merriman et al. 1990). Once dry, the mixture
228 was scanned from 2° to $15^\circ 2\theta$ with a $\text{CuK}\alpha$ Scintag X-1 X-ray powder diffractometer at the
229 University of Michigan, using a step size of $0.01^\circ 2\theta$. IC values were determined automatically
230 using the MacDiff software program. Samples were treated with ethylene glycol to evaluate the
231 presence of expandable clays (smectite), however no measurable effects were observed. To
232 account for sensitivity to sample preparation (i.e. differences in slurry thickness), each sample
233 was analyzed three times at different areas and an average of the three was used to represent the
234 grade of the sample.

235 *X-ray polytype quantification*

236 The crystallographic structure of illite also depends on the c-axis rotation of individual
237 packets. Polytypes are structural classes defined by the amount of rotation between neighboring
238 packets (Smith and Yoder, 1956). The two most commonly recognized illite polytypes are the
239 $1M_d$ and $2M_1$ illite polytypes. Described by Moore and Reynolds (1997), the $1M_d$ polytype is
240 characterized by a disordered, one packet monoclinic symmetry with irregularly rotating packets.
241 Unlike $1M_d$, the $2M_1$ polytype has a two packet monoclinic symmetry with a regular 120°
242 rotation of packets. The transition from disordered $1M_d$ to the ordered $2M_1$ polytype is the
243 result increasing metamorphic grade and it is highly correlated with illite crystallinity (Hunziker
244 et al., 1986).

245 **Sample preparation:** Random powder mounts were prepared for all three grain-size
246 fractions. The mounts were scanned from 16° to 39°2 θ , with a CuK α Scintag X-1 X-ray powder
247 diffractometer, using a step size of 0.05°2 θ . X-ray results are compared with end-member
248 patterns made using the program WILDFIRE© (Grathoff and Moore, 1996). Proportions of illite
249 polytypes for each size fraction were estimated by visually matching the measured XRD patterns
250 with end-member mixed patterns.

251 *TEM*

252 To visually characterize illite/muscovite crystal structures including grain-size,
253 expandable interlayers, and lattice dislocations, TEM analyses were performed on $\leq 2 \mu\text{m}$ clay
254 mineral separates. Clay separates were centrifuged to achieve the desired orientation prior to ion
255 milling. Electron microscopy was performed with a Phillips CM 12 scanning-transmission
256 electron microscope (STEM) with a Kevex Quantum solid-state detector. For this study, analyses
257 were made at 120 kV and 20 mA.

258

259 **RESULTS**

260 *Illite Crystallinity*

261 IC measurements of $\leq 2 \mu\text{m}$ size fractions from both fault samples and the footwall sample
262 all yield values consistent with anchizonal grade metamorphism (Table 1). Figure 5 shows
263 representative spectra for each of the three samples and its corresponding IC average. All of the
264 samples have peaks at 1nm, indicating the presence of illite/muscovite. 1 nm XRD peaks are
265 fairly narrow, without the presence of an initial ‘hump’ prior to the peak, indicating the lack (or

266 only trace presence) of expandable interlayers (Fig. 5). All three replicate analyses for each
267 sample lie within the anchizonal grade of metamorphism with calculated average values of 0.35,
268 0.38 and 0.36 \pm 0.02 for the fault center, fault margin and footwall respectively (Table 1). For each
269 sample, the difference in IC values is minor with a standard deviation of \sim 3%. The fact that all
270 three samples lie within the low anchizone indicates that the Champlain Thrust and Iberville Fm.
271 slates experienced peak metamorphic temperatures between 200 - 300°C.

272 X-ray polytype quantification of grain-size separates for each of the samples indicates a
273 mixture of 1M_d and 2M₁ illite grains in each of the grain-size fractions (Table 1 and DR. 1). All
274 three samples show an increase in the percentage of 2M₁ illite from the finest grain-size fraction
275 to the coarsest. 1M_d/2M₁ mixture results from polytype quantification are confirmed by TEM
276 observation of <2 μ m grain-size separates (DR. 1). TEM imaging indicates that the two fault
277 samples and the footwall sample are made up of well-crystallized white mica grains (Fig. 6A).
278 1M_d grains are thin (\sim 40-50 nm) with minor dislocations due to trace amounts of smectite
279 interlayers in illite-smectite packets and improper layer terminations (Fig. 6B and 6C). 2M₁
280 grains are significantly thicker (\sim 80-100 nm) and well crystallized. The development of 2M₁ at
281 the expense of 1M_d is the result of dissolution of 1M_d and crystallization of larger 2M₁ grains
282 due to tectonic stresses at temperatures \geq 200 °C (Merriman and Peacor, 1999). IC, X-ray
283 quantification and TEM analyses indicate that authigenic 2M₁ white mica from the Champlain
284 Thrust and Iberville Fm. may have grown at the expense of diagenetic 1M_d white mica. It is
285 likely they the samples contain a mixture of detrital and authigenic 2M₁ illite.

286

287 *⁴⁰Ar/³⁹Ar Geochronology*

288 $^{40}\text{Ar}/^{39}\text{Ar}$ vacuum encapsulated step-heating results are in Table 1 and illustrated in Fig 7.
289 For each sample, we will discuss the ^{39}Ar recoil fraction released when the tubes were broken,
290 the total gas age and retention age, and the maximum ages reached during step-heating.

291

292 ***Fault Center Sample***

293 For the sample collected from the center of the fault zone, the $<0.05\ \mu\text{m}$ grain-size had
294 the greatest fraction ($\sim 34\%$) of ^{39}Ar lost due to recoil while the coarsest fraction ($0.2\text{-}2\ \mu\text{m}$) lost
295 the least ($\sim 15\%$). The two finer size-fractions produced ‘hump-back’ shaped spectra that both
296 reach a maximum age of 385 Ma. The $0.2\text{-}2\ \mu\text{m}$ size fraction has a ‘stair-case’ shaped spectrum
297 that reaches a maximum age of 451 Ma recorded at higher temperatures. All three grain-size
298 fractions yield total gas ages that decrease with decreasing grain-size. Total gas ages range from
299 $326.8 \pm 0.9\ \text{Ma}$ in the $0.2 - 2\ \mu\text{m}$ size-fraction to $227.4 \pm 1.3\ \text{Ma}$ in the $<0.05\ \mu\text{m}$ fraction.
300 Retention ages for the <0.05 and $0.05 - 0.2\ \mu\text{m}$ size fractions produce ages of $336.8 \pm 1.5\ \text{Ma}$
301 and $338.6 \pm 1.2\ \text{Ma}$ respectively and the $0.2 - 2\ \mu\text{m}$ fraction yields an age of $376.4 \pm 1\ \text{Ma}$. This
302 is approximately 35 m.y. older than the finer fractions.

303

304 ***Boundary Sample***

305 In the sample collected near the contact with the hanging wall, the $<0.05\ \mu\text{m}$ grain-size
306 had the greatest fraction ($\sim 29\%$) of ^{39}Ar lost due to recoil while the coarsest fraction ($0.2\text{-}2\ \mu\text{m}$)
307 lost the least ($\sim 17\%$). All three grain-sizes have a ‘hump-back’ shape degassing spectrum that
308 have maximum age around 286 Ma for $0.05\text{-}0.2$ and $0.2\text{-}2\ \mu\text{m}$ size fractions and a maximum age

309 of 332 Ma for the $\leq 0.05 \mu\text{m}$ fraction. Similar to the center sample, total gas ages of the three
310 grain-size fractions at the boundary yield three different ages that decrease with grain-size from
311 $219.0 \pm 0.7 \text{ Ma}$ to $188.6 \pm 0.5 \text{ Ma}$ in the finest fraction. Regardless of grain size, each size
312 fraction from the boundary sample yields essentially the same retention age at $\sim 260 \text{ Ma}$.

313

314 ***Iberville Formation slates***

315 Slates of the Iberville Fm. sampled from the footwall of the Champlain Thrust yield
316 complex degassing patterns. With decreasing grain size, the percentage of ^{39}Ar that is lost due to
317 recoil increases from 16% in the $0.2\text{-}2 \mu\text{m}$ fraction to 37% in the $\leq 0.05 \mu\text{m}$ fraction. The step-
318 heating spectrum for the $0.2\text{-}2 \mu\text{m}$ size fraction is ‘humped’ shaped with a flat area around 400
319 Ma with a maximum age of 422 Ma. The ≤ 0.05 and $0.05\text{-}0.2 \mu\text{m}$ fractions have ‘stair-case’
320 shaped patterns that have maximum ages of 547 Ma and 501 Ma respectively. In the slate
321 sample, $^{40}\text{Ar}/^{39}\text{Ar}$ results yield a decrease in the total gas age with decreasing grain-size from
322 $324.91 \pm 1.15 \text{ Ma}$ in the coarsest fraction to $281.91 \pm 1.01 \text{ Ma}$ in the finest fraction. It has been
323 shown by many authors (e.g., Hower et al., 1963) that ages decrease with decreasing grain-size.
324 Retention ages typically decrease with decreasing grain size, however for illite separates from
325 the Iberville Fm. Slates, the retention ages actually increase with decreasing grain size. The
326 oldest age of $428.15 \pm 1.50 \text{ Ma}$ is recorded in the finest fraction, while the youngest retention age
327 of $380.45 \pm 1.33 \text{ Ma}$ is recorded in the coarsest fraction.

328

329 ***$^{40}\text{Ar}/^{39}\text{Ar}$ Modeling***

330 The Ar retention age model has been found to be very useful in constraining the timing of
331 clay formation both in conditions of hydrothermal alteration (Hall et al., 1997) and regional
332 metamorphism (Dong et al., 1997). The model corrects for loss of radiogenic ^{40}Ar (i.e. $^{40}\text{Ar}^*$) in
333 nature from the same sites that do not retain ^{39}Ar during neutron irradiation. Implicit in this age
334 model is that there is K in defect sites in the same concentration as in retentive sites and therefore
335 that portion of the total ^{39}Ar inventory should not be used in calculating an age. In essence, the
336 retention age corrects for the loss of $^{40}\text{Ar}^*$ that has taken place. In contrast to the retention age
337 model, the total gas age model assumes that there is no K in non-retentive sites. This age model
338 has been found to be most accurate for samples with a large proportion of expandable layer sites
339 (e.g., Dong et al., 2000; van der Pluijm et al., 2001; Haines and van der Pluijm, 2008).

340 From Table 1, it can be seen that neither the retention age model nor the total gas age
341 model gives consistent results. The total gas age model decreases with increasing fraction of ^{39}Ar
342 lost due to recoil while the retention age increases. Therefore, it appears that there has been some
343 loss of $^{40}\text{Ar}^*$ from non-retentive sites, but the retention age model apparently over-corrects for
344 this effect, likely because the non-retentive sites do not have K concentrations as high as for
345 retentive sites.

346 The results from Table 1 show that both end-member age models for the Iberville Fm.
347 converge toward an age of about 350 Ma as the fraction of ^{39}Ar lost due to recoil approaches
348 zero. This suggests that it may be possible to model formation of slaty cleavage by using a linear
349 combination of a function of both the retention and total gas ages. If all size fractions have the
350 same relative concentration of K f_d (radioactive K) in non-retentive defect sites, then it is
351 possible to estimate the expected $^{40}\text{Ar}^*/^{39}\text{Ar}_K$ ratio assuming that all size fractions closed to ^{40}Ar

352 loss from retentive sites at the same time. We will denote the neutron-fluence normalized ratio of
353 radiogenic ^{40}Ar to ^{39}Ar as r , where:

$$354 \quad r = J \frac{{}^{40}\text{Ar}^*}{{}^{39}\text{Ar}_K} = e^{\lambda t} - 1 \quad (\text{eq. 1})$$

355 Here J is the usual conversion factor based on analysis of standard minerals of known K-Ar age
356 and λ is the total decay constant for ^{40}K . Then the expected value of r_m (ratio of $^{40}\text{Ar}^*/^{39}\text{Ar}_K$) for
357 any given grain-size fraction can be written as:

$$358 \quad r_m = f_d (e^{\lambda t_R} - 1) + (1 - f_d) (e^{\lambda t_{TG}} - 1) \quad (\text{eq. 2})$$

359 where t_R and t_{TG} are the retention and total gas ages respectively. The value of f_d was estimated
360 by minimizing the error-weighted deviations of r_m for the three different grain size fractions. The
361 best-fit value of f_d is 0.4626 and the age derived from the optimal r_m value is 350.6 ± 1.2 Ma with
362 a χ^2 value of 1.39 and 2 degrees of freedom. We regard this as the best estimate of the age of
363 slaty cleavage formation in the Iberville formation.

364

365

366 **DISCUSSION**

367 *Age Model*

368 Illite crystallinity measurements of the Champlain fault samples and Iberville slates
369 indicate that the samples experienced anchizonal grade metamorphism. The anchizone is a
370 transitional zone between diagenesis and low-grade metamorphism (greenschist facies) in

371 metapelitic rocks that is associated with the loss of expandable interlayers and the transformation
372 of thin and poorly crystallized $1M_d$ to thick and well-crystallized $2M_1$ illite polymorphs
373 (Maxwell and Hower, 1967; Hunziker et al. 1986). X-ray quantification indicates that the fault
374 rocks and slates contain two modes of illite, thick authigenically produced $2M_1$ and thin
375 diagenetic $1M_d$ illite polymorphs. However, given the maximum age for the coarsest fraction
376 from the center samples, some samples may contain some detrital $2M_1$ illite. The transition from
377 late diagenetic to anchizonal grade is characterized by the growth of white mica by dissolution
378 and crystallization (i.e. Merriman et al., 1990; Jiang et al., 1997). The growth of authigenic white
379 mica is correlated with an increase in the thickness of crystallites and a decrease in the
380 proportion of crystal defects (Jiang et al., 1997). Therefore, the anchizone is synonymous with
381 the growth of thicker, defect-free grains that are able to retain ^{39}Ar and ^{40}Ar . Based on the illite
382 crystallinity values ($<0.42^\circ 2\theta$), polytype quantification results ($2M_1$ -rich), and TEM imaging
383 (thick illite packets), the retention age is the appropriate age model to apply to the fault samples
384 in this study.

385 *Fault Center Sample*

386 For the sample collected in the center of the Champlain thrust, retention ages for the two
387 finer grain-size fractions are similar in age, while the $0.2 - 2 \mu\text{m}$ fraction is ~ 35 my older. In
388 Figure 7, the degassing spectra from each the <0.05 and $0.05-0.2 \mu\text{m}$ grain-size fractions lie on
389 top of one another, indicating that the center sample either cooled below the illite/muscovite
390 closure temperature or crystallized new $2M_1$ illite grains around 336-338 Ma. The $0.2-2 \mu\text{m}$
391 grain-size degassing spectrum does not lie on top of the other two fractions, which indicates that
392 all ^{40}Ar was not completely degassed, or that there is a detrital influence. We propose, based on
393 the shapes of the $^{40}\text{Ar}/^{39}\text{Ar}$ degassing spectra for the three grain-sizes, that the center sample was

394 heated above the Ar closure temperature window to allow the finer fractions to completely reset.
395 The coarsest fraction did experience a significant amount of ^{40}Ar diffusive loss; however it was
396 not completely reset, and still contains older inherited ^{40}Ar .

397 The closure temperature for illite is not-well constrained. Low-grade metamorphism
398 studies (Hunziker et al. 1986, Merriman and Frey, 1999; Verdel et al., 2012) determined
399 approximate closure temperatures for the loss of ^{40}Ar to be between 250 to 350 °C. Experimental
400 studies by Harrison et al. (2009) have shown that hydrothermal treatment of muscovite (micron-
401 size) induced radiogenic ^{40}Ar loss that is revealed in $^{40}\text{Ar}/^{39}\text{Ar}$ step heating spectra. Illite is a K-
402 deficient white mica so it is assumed (in the absence of actual data) that it acts similar to
403 muscovite. Figure 8 shows the relationship between cooling rate and grain size on the closure
404 temperature of ^{40}Ar in muscovite. This plot utilizes the activation energy ($E = 63 \pm 7$ kcal/mol)
405 and frequency factor ($D_0 = 2.3 +70/-2.2$ cm²/s) reported by Harrison et al. (2009) and modeled
406 for a cylindrical geometry, which Hames and Bowring (1994) have shown to best represent the
407 diffusional pathways for micas. The grain-sizes used for this plot are the same that were analyzed
408 for this study. It is worth noting that the ^{40}Ar closure temperature for the two finer fractions have
409 closure temperatures largely <300 °C (Fig. 8). These temperatures are significantly less than the
410 ~350 °C closure temperature that is assumed for muscovite, due to smaller diffusion dimensions
411 (e.g., Hodges, 1991). It is also significant that the finest fraction (<0.05 μm) may begin losing
412 ^{40}Ar by ~240 °C. Illustrated in Figure 8, the center sample of the Champlain Thrust experienced
413 temperatures ~270-300 °C.

414

415 ***Boundary Sample***

416 For the sample collected at the boundary, all retention ages are essentially the same at
417 ~260 Ma. In Figure 7, the degassing spectra for each size fraction lie on top of one another,
418 indicating that the boundary sample either cooled or recrystallized around 260 Ma. Since the
419 coarsest grain-size fraction (0.2-2 μm) lost all of its inherited ^{40}Ar , temperatures must have been
420 above 300 $^{\circ}\text{C}$ for ^{40}Ar to diffuse from a 2 μm grain (Fig. 8).

421

422 *Interpretation of $^{40}\text{Ar}/^{39}\text{Ar}$ ages*

423 Determining if the $^{40}\text{Ar}/^{39}\text{Ar}$ geochronology ages are cooling, recrystallization or low-
424 grade metamorphic ages is difficult using bulk mineral separates. However, $^{40}\text{Ar}/^{39}\text{Ar}$ step-
425 heating experiments on various grain-size fractions, combined with X-ray diffraction analyses
426 and TEM imaging, allow us to understand the mechanisms involved in producing the age results
427 of this study. All three samples dated in this study lie within the anchizone, indicating that
428 thermal overprinting due to low-grade metamorphism had significant effects on the Ar results.
429 As stated above, the anchizone is characterized by the dissolution of thin and poorly crystallized
430 1M_d illite and crystallization of thick and well-crystallized 2M_1 illite polymorphs, indicating that
431 low-grade metamorphism occurred in the Champlain Thrust and Iberville Fm. slates. However,
432 X-ray quantification and TEM results show that the fault rocks and slates still contain a
433 significant amount of diagenetic 1M_d with minimal detrital 2M_1 illite, signifying that
434 crystallization of 2M_1 was not the only mechanism involved in the age results. Diagenetic and
435 detrital illite contains inherited ^{40}Ar , which increases the age of the sample being studied
436 (Hunziker et al., 1986; Dong et al., 2000). Therefore, isotopic loss of ^{40}Ar by diffusion needs to
437 occur in the 1M_d and 2M_1 illite grains to homogenize the Ar system. Both crystallization of 2M_1

438 illite and diffusion due to low-grade metamorphism occurred in the Champlain Thrust and
439 Iberville Fm.

440 *Timing of fault movement*

441 Based on stratigraphic relations, Rowley and Kidd (1981) proposed that thrusting along
442 the Champlain Thrust occurred during the Middle to Late Ordovician (late Caradocian, 461-449
443 Ma). $^{40}\text{Ar}/^{39}\text{Ar}$ retention ages obtained from $\leq 2\mu\text{m}$ clay separates in this study are significantly
444 younger than this accepted formation age of the fault. Results from this study indicate that either
445 the Champlain Thrust did not develop until the Mississippian, or initially formed during the Mid-
446 Ordovician Taconic Orogeny and was later deformed and metamorphosed during subsequent
447 tectonic events. We propose, based upon the new Ar retention and maximum ages presented in
448 this study, that the Champlain Thrust of western Vermont was initially formed during the
449 Taconic Orogeny and later experienced two additional deformation pulses.

450 Staircase shaped degassing spectra reflect a mixture of grains that contain variations in
451 age and Ar retention (Kirschner et al. 1996; Harrison and McDougall, 1999). The coarse (0.2-2
452 μm) grain-size fraction from the center of the Champlain Thrust yields a gently climbing
453 spectrum that reaches a maximum age of 451 Ma at the highest degassing temperature (Fig. 7).
454 The 451 Ma maximum age is in good agreement with the initial Mid to Late Ordovician
455 formation age proposed by Rowley and Kidd (1981), suggesting that this sample contains relict
456 illite grains that retain ages that record the initial development of the Champlain Thrust during
457 the Ordovician around 451 Ma.

458 Following the Taconic Orogeny, the L. Silurian – Carboniferous, Acadian-Neoacadian
459 Orogeny was the next major deformation event to affect the northern Appalachians (Robinson et

460 al., 1998; Hatcher, 2002, 2010). The Acadian-Neocadian caused major crustal shortening,
461 plutonism and high-temperature metamorphism due to the accretion of the Avalon terrane that is
462 primarily preserved in central New England (i.e. central Massachusetts and western New
463 Hampshire). $^{40}\text{Ar}/^{39}\text{Ar}$ results from the center of the Champlain Thrust fall within the window of
464 the Acadian-Neocadian Orogeny. We propose that Acadian-Neocadian deformation and
465 metamorphism caused clay mineral transformations and isotopic loss by ^{40}Ar diffusion of illite
466 grains in the Champlain Thrust at ~ 338 Ma. Ages younger than the timing of peak high-grade
467 Acadian metamorphism (~ 390 Ma, Robinson et al., 1998) are interpreted as representing cooling
468 ages as the result of Acadian-Neocadian loading and denudation (Harrison et al., 1989; Zen,
469 1991; McWilliams, 2008). It is likely that the 338 Ma and 336 Ma ages from the center of the
470 Champlain thrust represent the Acadian-Neocadian cooling of the fault zone through the closure
471 temperature by uplift and erosion due to rebound from a tectonically thickened crust (Harrison et
472 al., 1989).

473 Thermal effects of the L. Mississippian – Permian Alleghanian Orogeny of the northern
474 Appalachians are concentrated in southeastern New England (i.e. Connecticut, Rhode Island and
475 eastern Massachusetts). However, recent thermobarometry measurements, $^{40}\text{Ar}/^{39}\text{Ar}$ and U-Pb
476 monazite dating have identified late Paleozoic Alleghanian ages overprinting Acadian-
477 Neocadian features to the northwest (Moecher, 1999; Spear et al. 2007; Massey and Moecher,
478 2008; McWilliams, 2008). The Alleghanian orogeny is the result of the collision of previously
479 accreted terranes to the Laurentian margin with Gondwana to form the supercontinent Pangaea
480 (Hatcher, 2002, 2010). Each grain-size fraction from the boundary sample yields a retention age
481 ~ 260 Ma, within the age window of the Alleghanian Orogeny. We interpret these ages to
482 represent a complete thermal resetting overprinting of Acadian-Neocadian illites that is

483 localized along the boundary with the hanging-wall during the Alleghanian Orogeny, evidence of
484 which is found in that the fine grain-size fraction has a maximum age (332 Ma) similar to its
485 retention age (Fig. 7). Based on similar percentages of $1M_d$ and $2M_1$ polytypes in each grain-size
486 fraction for the two Champlain Thrust samples, this may indicate that the primary cause for
487 isotopic resetting was ^{40}Ar loss due to diffusion and that crystallization of new $2M_1$ grains was
488 minimal. It is our interpretation that these ages do not represent exhumation ages due to
489 extension and the break-up of Pangaea, since normal faulting did not occur until the Late Triassic
490 – Early Jurassic (Manspeizer et al., 1989).

491 *Timing of cleavage formation*

492 Slaty cleavage of the Taconic allochthonous and parautochthonous terranes is typically
493 interpreted to be an Ordovician structure that developed during the main regional deformation
494 and metamorphism associated with the Taconic Orogeny (Bosworth, 1980; Rowley, 1983;
495 Bosworth and Rowley, 1984). Several attempts have been made using geochronology (K-Ar and
496 $^{40}\text{Ar}/^{39}\text{Ar}$) to establish the timing of cleavage formation in the Taconic allochthonous and
497 parautochthonous zones, but these have been met with minimal success (Harper, 1968; Cady,
498 1969; Sutter et al., 1985; Chan et al. 2001). Early studies used K-Ar of whole rock and bulk
499 muscovite separates and these provided a wide range of ages from the Late Ordovician to the
500 Mid Devonian with large errors (Harper, 1968; Cady, 1969; Sutter et al., 1985). Variations in age
501 are likely the result of a mixture of detrital grains that contain an inherited Ar signature related to
502 their source rock and authigenically produced mica grains due to low-grade metamorphism.
503 Laser-probe ages by Chan et al. (2001) provided tighter constraints in ages between 360-310 Ma
504 with a mean age of 345 Ma, but the errors on their results were large. Using the linear
505 combination of retention age and total gas age with a similar concentration of K in non-retentive

506 sites we were able to obtain an age of 350.6 ± 1.2 Ma for the formation of slaty cleavage and
507 low-grade metamorphism due to the Acadian-Neoacadian orogeny. This Early Mississippian age
508 for the formation of slaty cleavage in the Iberville formation is consistent with the Mississippian
509 age for metamorphism and ^{40}Ar loss from the center of the Champlain thrust.

510 **Conclusion**

511 In this study of fault-related phyllites and nearby slates in northern Vermont, we conclude
512 that:

513 1) For samples within the anchizone, the retention age model should be applied to bulk-
514 separate vacuum encapsulated $^{40}\text{Ar}/^{39}\text{Ar}$ data. This model accounts for diffusive and recoil losses
515 of ^{40}Ar in nature that are unaccounted for by traditional total gas ages.

516 2) $^{40}\text{Ar}/^{39}\text{Ar}$ step-heating experiments in combination with illite crystallinity, x-ray
517 polytype quantification and TEM imaging indicate that illite grains in the Champlain Thrust and
518 Iberville Fm. slates experienced two mechanisms which produce younger than expected Ar ages:
519 1) the dissolution of diagenetic 1M_d illite and crystallization of 2M_1 illite; 2) a thermal overprint
520 and diffusive loss of ^{40}Ar of 1M_d illite due to low-grade metamorphism.

521 3) After the Champlain Thrust formed during the Mid-to-Late Ordovician (~ 450 Ma), it
522 was later affected by two phases of deformation and metamorphism: the Acadian-Neoacadian
523 Orogeny at ~ 340 Ma and a later phase that was localized along the contact with the hanging wall
524 ~ 260 Ma, coinciding with the Alleghanian Orogeny.

525 4) Using a linear combination of retention age and total gas ages with a similar
526 concentration of K in non-retentive sites, an age of 350 Ma is obtained for the formation of slaty
527 cleavage in the Iberville Formation at Mt. Philo.

528 **Acknowledgments**

529 The authors like to thank Jon Kim, Keith Klepeis and Laura Webb for thought provoking
530 discussions and assistance in the field. We also like to thank Anja Schleicher for support with
531 TEM characterization and Charles Verdel for providing comments and ideas on an early draft of
532 the manuscript. Research was supported by the National Science Foundation, EAR-0738435 (to
533 BvdP) and grants from the GDL Foundation and a Turner Fellowship from the University of
534 Michigan (to TMO).

535 **References**

- 536 Bird, J.M., and Dewey, J.F., 1970, Lithosphere plate-continental margin tectonics and the
537 evolution of the Appalachian orogeny: Geological Society of America Bulletin, v. 88, p.
538 1031-1060.
- 539 Bosworth, W., and Rowley, D.B., 1984, Early obduction-related deformation features of the
540 Taconic Allochthon: Analogy with structures observed in modern trench environments:
541 Geological Society of America Bulletin, v. 95, p. 559-567.
- 542 Bradley, D.C., 1989, Taconic plate kinematics as revealed by foredeep stratigraphy, Appalachian
543 orogeny: Tectonics, v. 8, p. 1037-1049.
- 544 Cady, W., 1969, Regional tectonic synthesis of northwestern New England and adjacent Quebec:
545 Geological Society of America Memoir, v. 120, 181 p.
- 546 Chan, Y.C., Crespi, J. M., and Hodges, K.V., 2001, Dating cleavage formation in slates, and
547 phyllites with $^{40}\text{Ar}/^{39}\text{Ar}$ laser microprobe: An example from the western New England
548 Appalachians, U.S.A.: Terra Nova, v. 12, p. 264-271.
- 549 Cosca, M., Stunitz, H., Bourgeix, A., and Lee, J.P., 2011, $^{40}\text{Ar}^*$ loss in experimentally deformed
550 muscovite and biotite with implications for $^{40}\text{Ar}/^{39}\text{Ar}$ geochronology of naturally
551 deformed rocks: Geochimica et Cosmochimica Acta, v. 75, 7759-7778.

- 552 Doll, C.G., Cady, W.M., Thompson, J.B., Jr., and Billings, M.P., 1961, Centennial geologic map
553 of Vermont: Montpelier, Vermont Geological Survey, 1 sheet, scale 1:250,000.
- 554 Dong, H., Hall, C.M., Peacor, D.R., and Halliday, A.N., 1995, Mechanism of argon retention in
555 clays revealed by later ^{40}Ar - ^{39}Ar dating: *Science*, v. 267, p. 355-359.
- 556 Dong, H., Hall, C.M., Halliday, A.N., Peacor, D.R., Merriman, R.J., and Roberts, B., 1997,
557 $^{40}\text{Ar}/^{39}\text{Ar}$ of Late Caledonian (Acadian) metamorphism and cooling of K-bentonites and
558 slates from the Welsh Basin, U.K.: *Earth and Planetary Science Letters*, v. 150, p. 337-
559 351.
- 560 Dong, H., Hall, C.M., Peacor, D.R., Halliday, A.N., and Peacor, D.R., 2000, Thermal $^{40}\text{Ar}/^{39}\text{Ar}$
561 separation of diagenetic from detrital illitic clays in Gulf Coast shales: *Earth and*
562 *Planetary Science Letters*, v. 175, 309-325.
- 563 Dunlap, W.J., 1997, Neocrystallization or cooling? $^{40}\text{Ar}/^{39}\text{Ar}$ ages of white micas from low-
564 grade mylonites: *Chemical Geology*, v. 143, p. 181-203.
- 565 Eberl, D.D., and Velde, B., 1989, Beyond the Kubler index: *Clay Minerals*, v. 24, p. 571-577.
- 566 Emmons, E., 1842, *Geology of New York, Part II; Survey of the Second Geological District:*
567 *Albany*, 437 p.
- 568 Frey, M., 1987, Very low-grade metamorphism of elastic sedimentary rocks, *in* Frey, M., ed.,
569 *Low temperature metamorphism*, New York, Chapman & Hall, p. 9-58.
- 570 Grathoff, G.H., and Moore, D.M., 1996, Illite polytype quantification using WILDFIRE
571 calculated X-ray diffraction patterns: *Clays and Clay Minerals*, v. 44, p. 835-842.
- 572 Haines, S.H., and van der Pluijm, B.A., 2008, Clay quantification and Ar-Ar dating of synthetic
573 and natural gouge: Application to the Miocene Sierra Mazatán detachment fault, Sonora,
574 Mexico: *Journal of Structural Geology*, v. 30, p. 525-538.
- 575 Hall, C.M., Higuera, P.L., Kesler, S.E., Lunar, R., Dong, H., and Halliday, A.N., 1997, Dating
576 of alteration episodes related to mercury mineralization in the Almadén district, Spain:
577 *Earth and Planetary Science Letters*, v. 148, p. 1092-1104.
- 578 Hall, C.M., Kesler, S.E., Simon, G., and Fortuna, J., 2000, Overlapping Cretaceous and Eocene
579 alteration, Twin Creeks Carlin-type deposit, Nevada: *Economic Geology*, v. 95, p. 1739-
580 1752.
- 581 Hames, W.E., and Bowring, S.A., 1994, An empirical evaluation of the Ar diffusion geometry in
582 muscovite: *Earth and Planetary Science Letters*, v. 124, p. 161-167.

- 583 Harper, C.T., 1968, Isotopic ages from the Appalachians and their tectonic significance:
584 Canadian Journal of Earth Science, v. 5, p. 49-59.
- 585 Harrison, T.M., Spear, F.S., and Heizler, M.T., 1989, Geochronologic studies in central New
586 England II: Post-Acadian hinged and differential uplift: *Geology*, v. 17, p. 185-189.
- 587 Harrison, T.M., C  lerier, J., Aikman, A.B., Hermann, J., and Heizler, M.T., 2009, Diffusion of
588 ⁴⁰Ar in muscovite: *Geochimica et Cosmochimica Acta*, v. 73, p. 1039-1051.
- 589 Hatcher, R.D., Jr., 2002, Alleghanian (Appalachian) orogeny, a product of zipper tectonics:
590 Rotational transpressive continent-continent collision and closing of ancient oceans along
591 irregular margins, *in* Mart  nez Catal  n, J.R., Hatcher, R.D. Jr, Arenas, R., and D  az
592 Garc  a, F., eds., Variscan-Appalachian dynamics: The building of the late Paleozoic
593 basement: Boulder, Colorado, Geological Society of America Special Paper 364, p. 199-
594 208.
- 595 Hatcher, R.D., Jr., 2010, The Appalachian orogeny: A brief summary, *in* Tollo, R.P.,
596 Bartholomew, M.J., Hibbard, J.P., and Karabinos, P.M., eds., From Rodinia to Pangea:
597 The Lithotectonic Record of the Appalachian Region: Geological Society of America
598 Memoir 206, p. 1-19, doi: 10.1130/2010.1206(01).
- 599 Hawley, D., 1957, Ordovician shales and submarine slide breccias of northern Champlain Valley
600 in Vermont: *Geological Society of America Bulletin*, v. 68, p. 55-94.
- 601 Hnat, J.S., 2009, Kinematic and temporal evolution of the southern Appalachian foreland fold-
602 thrust belt: Constraints from structural, magnetic and radiometric analyses [Ph.D. thesis]:
603 Ann Arbor, University of Michigan, 286 p.
- 604 Hodges, K.V., 1991, Pressure-temperature-time paths: *Annual Review in Earth and Planetary*
605 *Science*, v. 19, p. 207-236.
- 606 Hower, J., Hurley, P.M., Pinson, W.H., and Fairbairn, H.W., 1963, The dependence of K-Ar age
607 on mineralogy of various particle size ranges in a shale: *Geochimica et Cosmochimica*
608 *Acta*, v. 27, p. 405-410.
- 609 Hunziker, J.C., Frey, M., Clauer, N., Dallmeyer, R.D., Friedrichsen, H., Flehmig, W.,
610 Hochstrasser, K., Roggwiler, P., and Schwander, H., 1986, The evolution of illite to
611 muscovite: Mineralogical and isotopic data from the Glarus Alps, Sitzerland:
612 *Contributions to Mineralogy and Petrology*, v. 92, p. 157-180.
- 613 Hurley, P.M., Hunt, J.M., Pinson, W.H., and Fairbairn, H.W., 1963, K-Ar age values on the clay
614 fractions in dated shales: *Geochimica et Cosmochimica Acta*, v. 27, p. 279-284.
- 615 Jaboyedoff, M., Bussy, F., K  bler, B., and Th  lin, P., 2001, Illite "crystallinity" revisited: *Clays*
616 *and Clay Minerals*, v. 49, p. 156-167.

- 617 Jiang, W.T., Peacor, D.R., Árkai, P., Tóth, M., and Kim, J.W., 1997, TEM and XRD
618 determination of crystallite size and lattice strain as a function of illite crystallinity in
619 pelitic rocks: *Journal of Metamorphic Geology*, v. 15, p. 267-281.
- 620 Karabinos, P., Sampson, S.D., Hepburn, J.C., and Stoll, H.M., 1998, Taconian orogeny in the
621 New England Appalachians, collision between Laurentia and the Shelburne Falls arc:
622 *Geology*, v. 26, p. 215-218.
- 623 Kirschner, D.L., Cosca, M.A., Masson, H., and Hunziker, J.C., 1996, Staircase $^{40}\text{Ar}/^{39}\text{Ar}$
624 spectra of fine-grained white mica: timing and duration of deformation and empirical
625 constraints on argon diffusion: *Geology*, v. 24, p. 747-750.
- 626 Kisch, H.J., 1983, Mineralogy and petrology of burial diagenesis (burial metamorphism) and
627 incipient metamorphism in clastic rocks: *in* Larsen, G., and Chilingar, G.V., eds.,
628 *Diagenesis in sediments and sedimentary rocks*, Vol. 2, Amsterdam, Elsevier, p. 289-493.
- 629 Kisch, H.J., 1991, Illite crystallinity: recommendations on sample preparation, X-ray diffraction
630 settings, and interlaboratory samples: *Journal of Metamorphic Geology*, v. 9, p. 665-670.
- 631 Kisch, H.J., and Frey, M., 1987, Appendix: effect of sample preparation on the measured 10 \AA
632 peak width of illite ("illite crystallinity"): *in* Frey, M., ed., *Low temperature*
633 *metamorphism*, New York, Chapman & Hall, p. 301-304.
- 634 Kligfield, R., Hunziker, J.C., Dallmeyer, R.D., and Schamel, S., 1986, Dating of deformation
635 phases using K/Ar and $^{40}\text{Ar}/^{39}\text{Ar}$ techniques: Results from the Northern Apennines:
636 *Journal of Structural Geology*, v. 8, p. 781-798.
- 637 Kübler, B., La cristallinité de l'illite et les zones tout à fait supérieures du métamorphisme, *in*
638 *Etages Tectoniques*, Colloque de Neuchâtel 1966, Université Neuchâtel, à la Baconnière,
639 Neuchâtel, Switzerland.
- 640 Kübler, B., and Jaboyedoff, M., 2000, Illite crystallinity: *Comptes Rendus de l'Académie des*
641 *Sciences*, v. 331, p. 75-89.
- 642 Manspeizer, W., deBoer, J., Costain, J. K, Froelich, A. J, Çoruh, C., Olsen, P. E., McHone, G. J.,
643 Puffer, J. H., and Prowell, D.C., 1989, Post-Paleozoic activity, *in* Hatcher, R. D. Jr.,
644 Thomas, W. A., and Viele, G. W., eds., *The Appalachian-Oachita Orogen in the United*
645 *States: Boulder Colorado*, Geological Society of America, *The Geology of North*
646 *America*, v. F2, p. 319-384.
- 647 Maxwell, D.T., and Hower, J., 1967, High-grade diagenesis and low-grade metamorphism of
648 illite in the Precambrian Belt Series: *American Mineralogist*, v. 52, p. 843-857.

- 649 Merriman, R.J., and Frey, M., 1999, Pattern of very low-grade metamorphism in metapelitic
650 rocks, *in* Frey, M., and Robinson, D., eds., *Low-Grade Metamorphism*, Blackwell
651 Science, Oxford, UK, p. 61-107.
- 652 Merriman, R.J., and Peacor, D.R., 1999, Very low-grade metapelites: mineralogy, microfabrics
653 and measuring reaction progress, *in* Frey, M., and Robinson, D., eds., *Low-Grade*
654 *Metamorphism*, Blackwell Science, Oxford, UK, p. 10-60.
- 655 Merriman, R.J., Roberts, B., and Peacor, D.R., 1990, A transmission electron microscope study
656 of white mica crystallite size distribution in a mudstone to slate transitional sequence,
657 North Wales, UK: *Contribution to Mineralogy and Petrology*, v. 106, p. 27-40.
- 658 Moecher, D.P., 1999, The distribution, style, and intensity of Alleghanian metamorphism in
659 south-central New England: Petrologic evidence from the Pelham and Willimantic
660 domes: *Journal of Geology*, v. 107, p. 449-471.
- 661 Moore, D.M., and Reynolds, R.C., 1997, X-ray diffraction and the identification and analysis of
662 clay minerals, 2nd edition: New York, Oxford University Press, 378 p.
- 663 Mosher, S., 1983, Kinematic history of the Narragansett basin, Massachusetts and Rhode Island:
664 Constraints on late Paleozoic plate reconstruction: *Tectonics*, v. 2, p. 327-344.
- 665 Mulch, A., Cosca, M.A., and Handy, M.R., 2002, In-situ UV-laser $^{40}\text{Ar}/^{39}\text{Ar}$ geochronology of
666 a micaceous mylonite—an example of defect-enhanced argon loss: *Contributions to*
667 *Mineralogy and Petrology*: v. 142, p. 738-752.
- 668 Ratcliffe, N.M., Hames, W.E., and Stanley, R.S., 1998, Interpretation of ages of arc magmatism,
669 metamorphism, and collisional tectonics in the Taconian orogeny of western New
670 England: *American Journal of Science*, v. 298, p. 791-797.
- 671 Reuter, A., and Dallmeyer, R.D., 1987, $^{40}\text{Ar}/^{39}\text{Ar}$ dating of cleavage formation in tuffs during
672 anchizonal metamorphism: *Contributions to Mineralogy and Petrology*, v. 97, p. 352-360.
- 673 Reynolds, M.W., 1963, Potassium-rubidium ratios and polymetamorphism in illites and
674 microclines from the clay size fractions of Proterozoic carbonate rocks: *Geochimica et*
675 *Cosmochimica Acta*: v. 27, p. 1097-1112.
- 676 Robinson, P., Tucker, R.D., Bradley, D., Berry, H.N., IV, and Osberg, P.H., 1998, Paleozoic
677 orogens in New England, U.S.A.: *Geologiska Foreningen I Stockholm Forhandlingar*
678 (GFF), v. 120, p. 119-148.
- 679 Rowley, D.B., and Kidd, W.S.F., 1981, Stratigraphic relationships and detrital composition of
680 the medial Ordovician flysch of western New England: Implications for the tectonic
681 evolution of the Taconic orogeny: *Journal of Geology*, v. 89, p. 199-218.

- 682 Rowley, D.B., 1982, New methods for estimating displacements of thrust faults affecting
683 Atlantic type shelf sequences: With an application to the Champlain thrust, Vermont:
684 Tectonics, v. 1, p. 369-388.
- 685 Samson, S.D., and Alexander, E.C., 1987, Calibration of the interlaboratory ^{40}Ar - ^{39}Ar dating
686 standard, MMhb-1: Chemical Geology, v. 66, p. 27-34, doi:10.1016/0168-
687 9622(87)90025-X.
688
- 689 Smith, J., and Yoder, H., 1956, Experimental and theoretical studies of the mica polymorphs:
690 Mineralogical Magazine, v. 31, p. 209-231.
691
- 692 Sutter, J.F., Ratcliffe, N.M., and Mukasa, S.B., 1985, $^{40}\text{Ar}/^{39}\text{Ar}$ and K-Ar data bearing on the
693 metamorphic and tectonic history of western New England: Geological Society of
694 America Bulletin, v. 96, p. 123-136.
695
- 696 Stanley, R.S., and Sarkenesian, A., 1972, Analysis and chronology of structures along the
697 Champlain Thrust west of the Hinesburg Synclinorium, in Doolan, D.L., and Stanley,
698 R.S., eds., Annual Meeting of the New England Geological Conference, 64th, Burlington,
699 Vermont, Guidebook for field trips in Vermont, p. 117-149.
700
- 701 Stanley, R.S., and Ratcliffe, N.M., 1985, Tectonic synthesis of the Taconian orogeny in western
702 New England: Geological Society of America Bulletin, v. 96, p. 1227-1250.
703
- 704 Stanley, R.S., 1987, The Champlain thrust fault, Lone Rock Point, Burlington, Vermont: in Roy,
705 D.C., eds., Northeastern Section of the Geological Society of America Centennial Field
706 Guide, v. 5, p. 225-228.
707
- 708 Tucker, R.D., and Robinson, P., 1990, Age and setting of the Bronson Hill magmatic arc: a re-
709 evaluation based on U-Pb zircon ages in southern New England: Geological Society of
710 America Bulletin, v. 102, p. 1404-1419.
- 711 Turner G., and Cadogan, P., 1974, Possible effects of ^{39}Ar recoil in ^{40}Ar - ^{39}Ar dating:
712 Proceedings of the 5th Annual Lunar and Planetary Science Conference, p. 1601-1615.
713
- 714 van der Pluijm, B.A., Hall, C.M., Vrolijk, P., Peavear, D.R., and Covey, M., 2001, The dating of
715 shallow crustal faults in the Earth's crust: Nature, v. 412, p. 172-174.
716
- 717 van der Pluijm, B.A., Vrolijk, P.J., Pevear, D.R., Hall, C.M. and Solum, J.G., 2006, Fault dating
718 in the Canadian Rocky Mountains: Evidence for late Cretaceous and early Eocene orogenic
719 pulses. Geology, v. 34, p. 837-840.
720
- 721 van Staal, C.R., 2007, Pre-Carboniferous tectonic evolution and metallogeny of the Canadian
722 Appalachians, in Goodfellow, W.D., ed., Mineral deposits of Canada: A synthesis of major
723 deposit-types, district metallogeny, the evolution of geological provinces, and exploration
724 methods: Geological Association of Canada, Mineral Deposit Division, Special Publication,
725 v. 5, p. 793-818.

726
727 Verdel, C., Niemi, N. and van der Pluijm, B.A., 2011. Variations in the illite-muscovite
728 transition related to metamorphic conditions and detrital muscovite content: Insight from the
729 Paleozoic passive margin of the S.W. US: *Journal of Geology*, v. 4, p. 419-437.
730
731 Verdel, C., van der Pluijm, B.A. and Niemi, N., 2012, Variation of illite/muscovite $^{40}\text{Ar}/^{39}\text{Ar}$
732 age spectra during progressive low-grade metamorphism: An example from the US
733 Cordillera: *Contributions to Mineralogy and Petrology*, published on-line on April 30, 2012,
734 doi: 10.1007/s00410-012-0751-7.
735
736 Warr, L.N., and Nieto, F., 1998, Crystallite thickness and defect density of phyllosilicates in low-
737 temperature metamorphic pelites: a TEM and XRD study of clay mineral crystallinity-
738 index standards: *Canadian Mineralogist*, v. 36, p. 1453-1474.

739 Warr, L.N., and Rice, A.H.N., 1994, Interlaboratory standardization and calibration of clay
740 mineral crystallinity and crystallite size data: *Journal of Metamorphic Geology*, v. 12, p.
741 141-152.

742 West, D.P., Lux, D.R., 1993, Dating mylonitic deformation by the ^{40}Ar - ^{39}Ar method: An
743 example from the Norumbega Fault Zone, Maine: *Earth and Planetary Science Letters*, v.
744 120, p. 221-237.

745 Wintsch, R.P., Kunk, M.J., Boyd, J.L., and Aleinikoff, J.N., 2003, P-T-t paths and differential
746 Alleghanian loading and uplift of the Bronson Hill terrane south central New England:
747 *American Journal of Science*, v. 303, p. 410-446.

748 Yang, C., and Hesse, R., 1991, Clay minerals as indicators of diagenetic and anchimetamorphic
749 grade in an overthrust belt, external domain of southern Canadian Appalachians:
750 *Canadian Mineralogist*, v. 26, p. 211-231.

751 Yoder, H.S., and Euster, H.P., 1955, Synthetic and natural muscovites; *Geochimica et*
752 *Cosmochimica Acta*, v. 8, p. 225-280.

753 Zen, E-An, 1967, Time and space relationships of the Taconic allochthon and autochthon:
754 *Geological Society of America Special Paper 97*, 107 p.

755 Zen, E-An, 1972, Some revisions in the interpretation of the Taconic allochthon in west-central
756 Vermont: *Geological Society of America Bulletin*, v. 72, p. 2573-2588.

757
758
759

759

760 Figure captions

761 Figure 1: Lithotectonic map of the Taconic fold-thrust belt of western New England, showing the
762 location of the Champlain Thrust and Mt. Philo (circle). Modified from Lim et al., 2005.

763

764 Figure 2: Generalized geologic map portraying the stratigraphy and structures near Burlington,
765 VT. Samples of the Champlain Thrust for this study were collected from Lone Rock
766 Point, located along the shore of Lake Champlain. Stratigraphic contacts and faults
767 adapted from Doll, 1961.

768

769 Figure 3: Outcrop patterns and structures of the Champlain Thrust at Lone Rock Point and
770 Iberville Fm. at Mt. Philo. A) Exposure of the thick fault zone of the Champlain Thrust
771 along Lake Champlain in contact with the Dunham Dolomite in the hanging wall. B)
772 Outcrop of the center of the Champlain thrust with thick black phyllosilicate-rich layers
773 interlayered with deformed carbonate veins. C) Isoclinal fold and boudinaged carbonate
774 vein located in the center. D) C-C' shear fabric with a westward vergence localized along
775 the boundary of the Champlain Thrust with the overlying Dunham Dolomite. E) Slaty
776 cleavage of the Iberville Fm.

777

778 Figure 4: A) Polished hand-sample slab, from the boundary of the thrust, containing deformed
779 asymmetric carbonate porphyroclasts and stretched veins. B) Highly twinned calcite
780 grains located within carbonate porphyroclasts. C) Quartz grain showing low-temperature
781 plastic deformational structures, including undulose extinction and the formation of sub-
782 grain.

783

784 Figure 5: Representative XRD measurements from each sample that displays the 1 nm (10 Å)
785 illite peak and corresponding averaged illite crystallinity results.

786

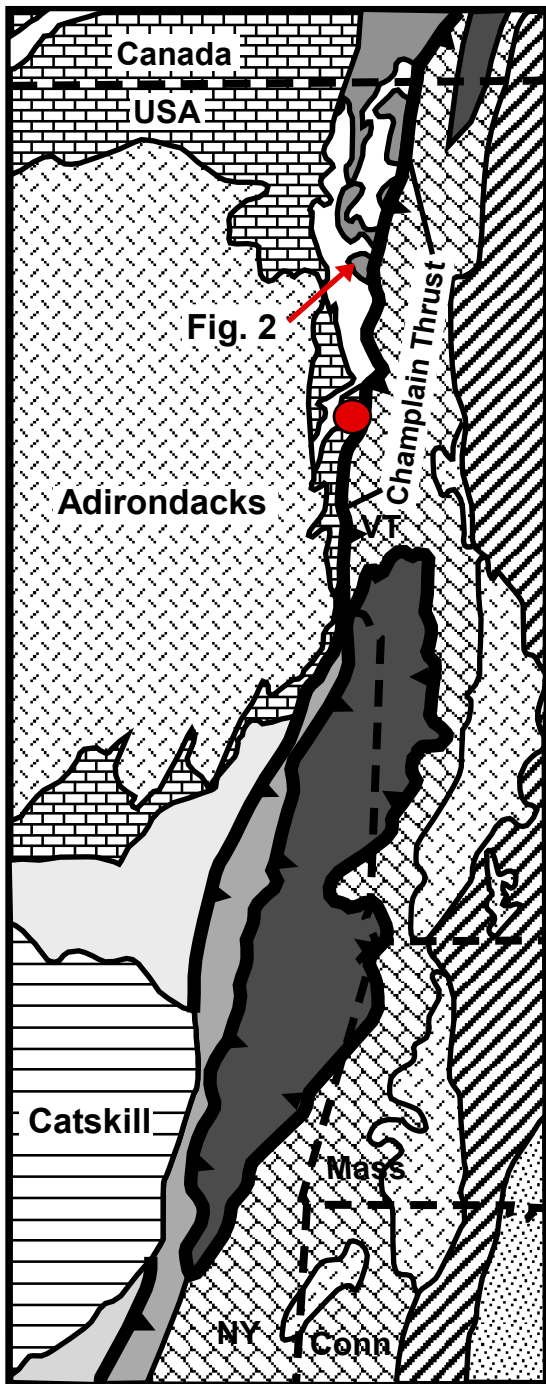
787 Figure 6: TEM images. A) Thick and well crystallized 2M₁ illite polytype. B) Poorly crystallized
788 1M_d illite polytype. C) Improper layer termination in 1M_d illite.

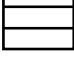







789

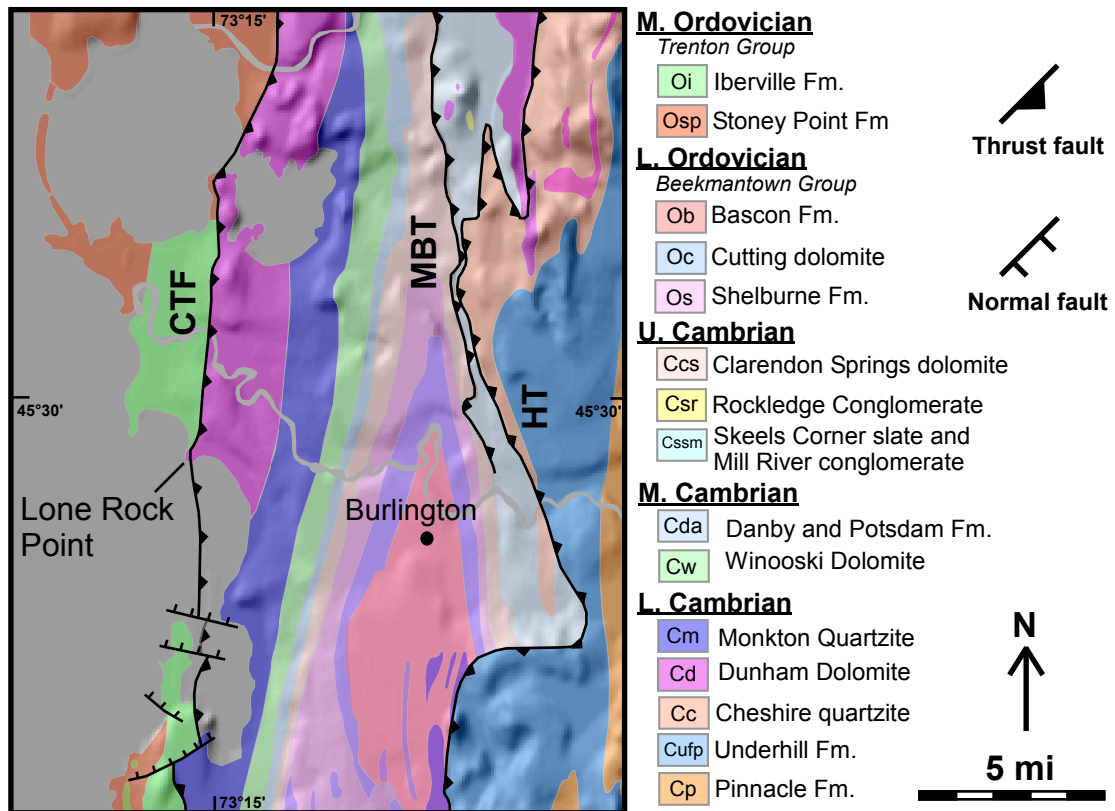
790 Figure 7: $^{40}\text{Ar}/^{39}\text{Ar}$ step-heating results <0.05, 0.05-0.2, and 0.2-2 μm grain-size fractions for
791 Champlain Thrust and Iberville Fm. slates.

792

793 Figure 8: Variation of closure temperature with cooling rate and grain-size fractions used for this
794 study.



-  Mesozoic rift fill
 -  Devonian Sequence
 -  Silurian-Devonian metasediments
 -  Taconic Allochthon
 -  Undeformed/deformed Ordovician Flysch
 -  Authochthonous/parautochthonous Cambrian-Ordovician shelf sequence
 -  Middle Proterozoic crystalline basement
-  50 km
-  Location of Mt. Philo

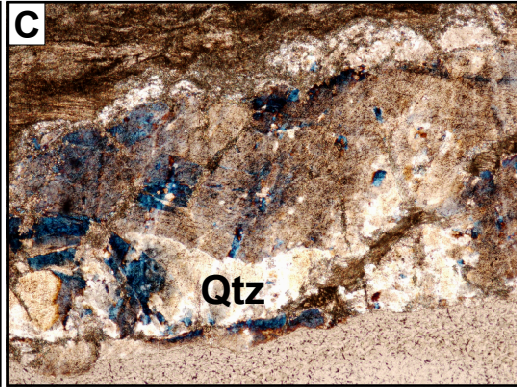
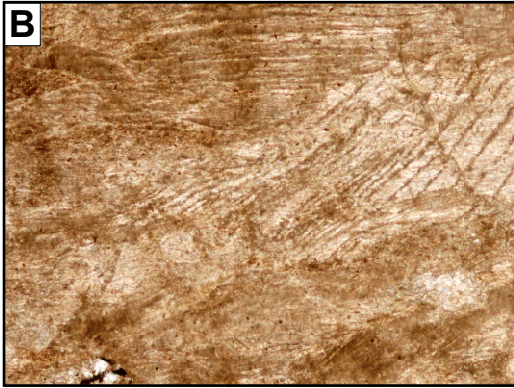
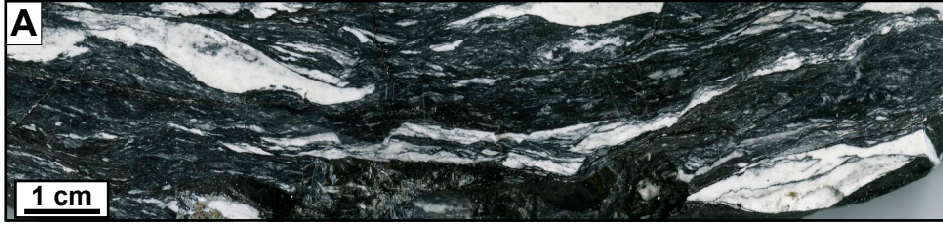


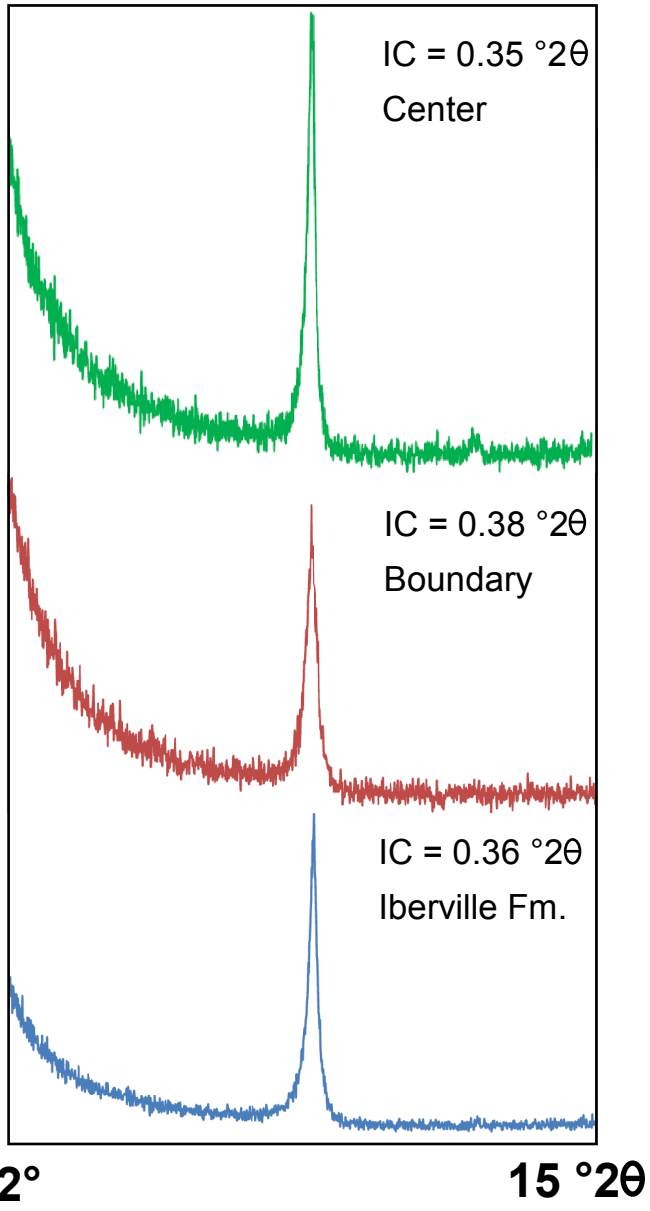
CTF = Champlain Thrust Fault

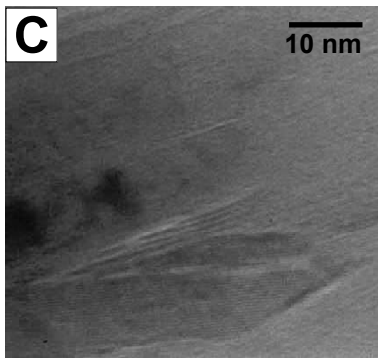
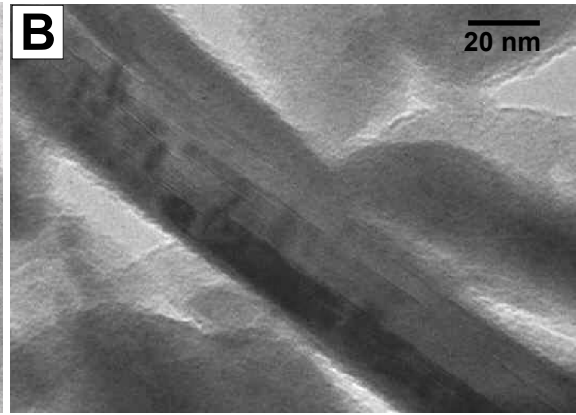
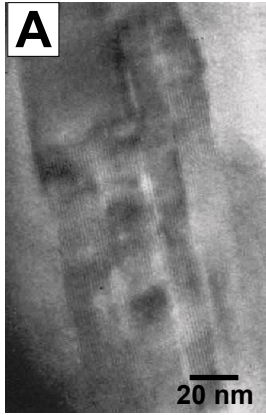
MBT = Muddy Brook Thrust

HT = Hinesburg Thrust

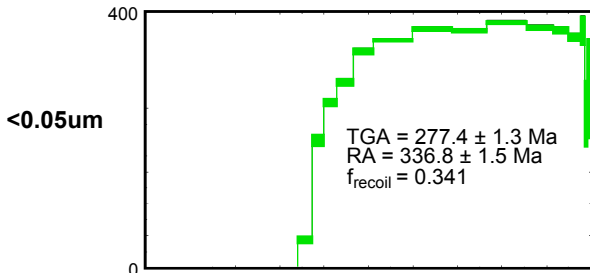




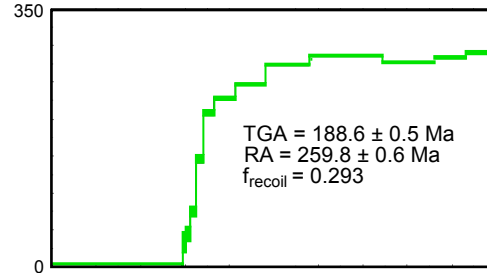




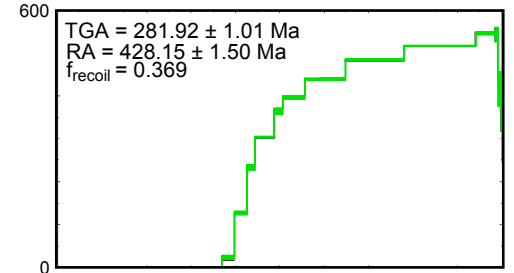
TOQ51204_center



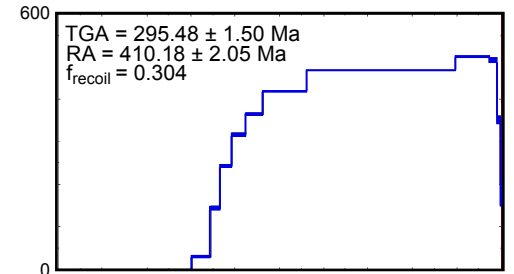
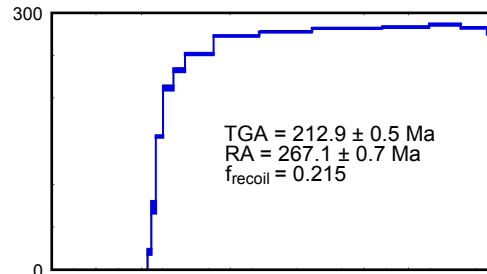
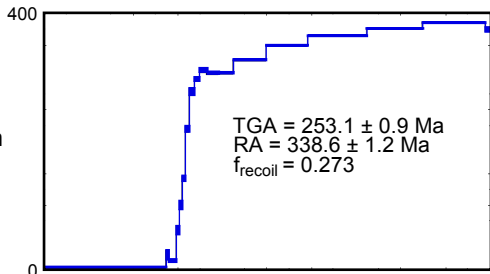
TOQ51204_margin



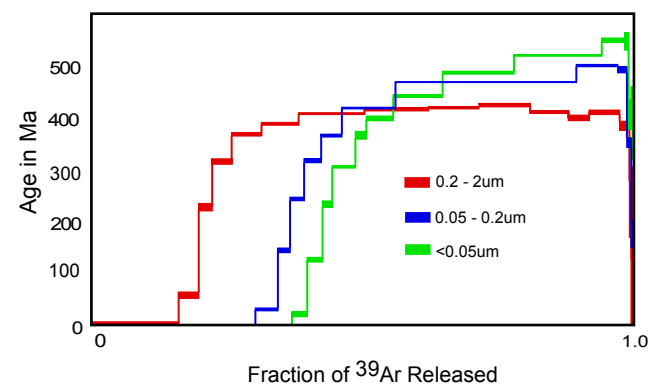
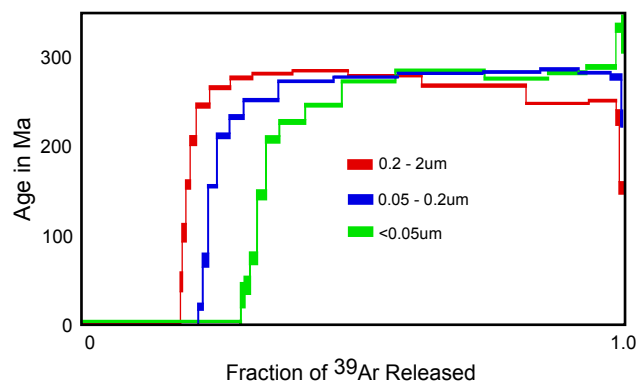
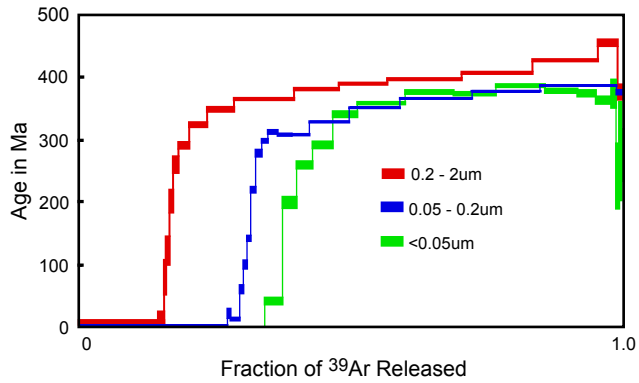
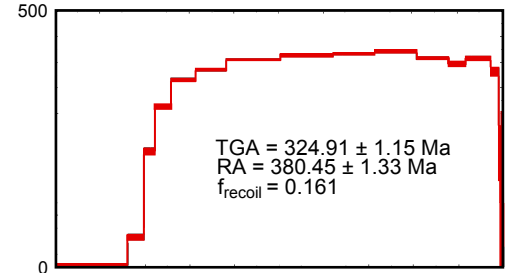
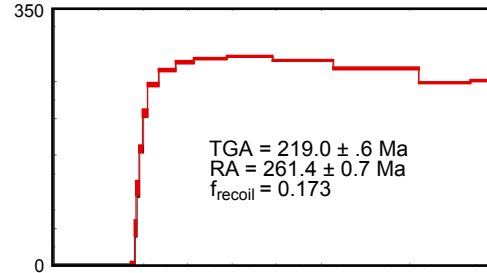
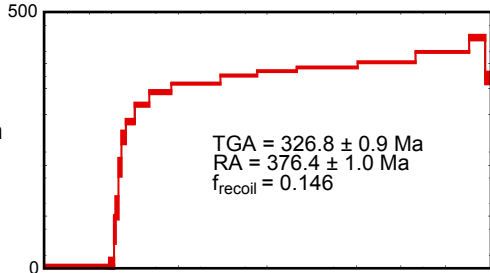
TOV52501 (slate)

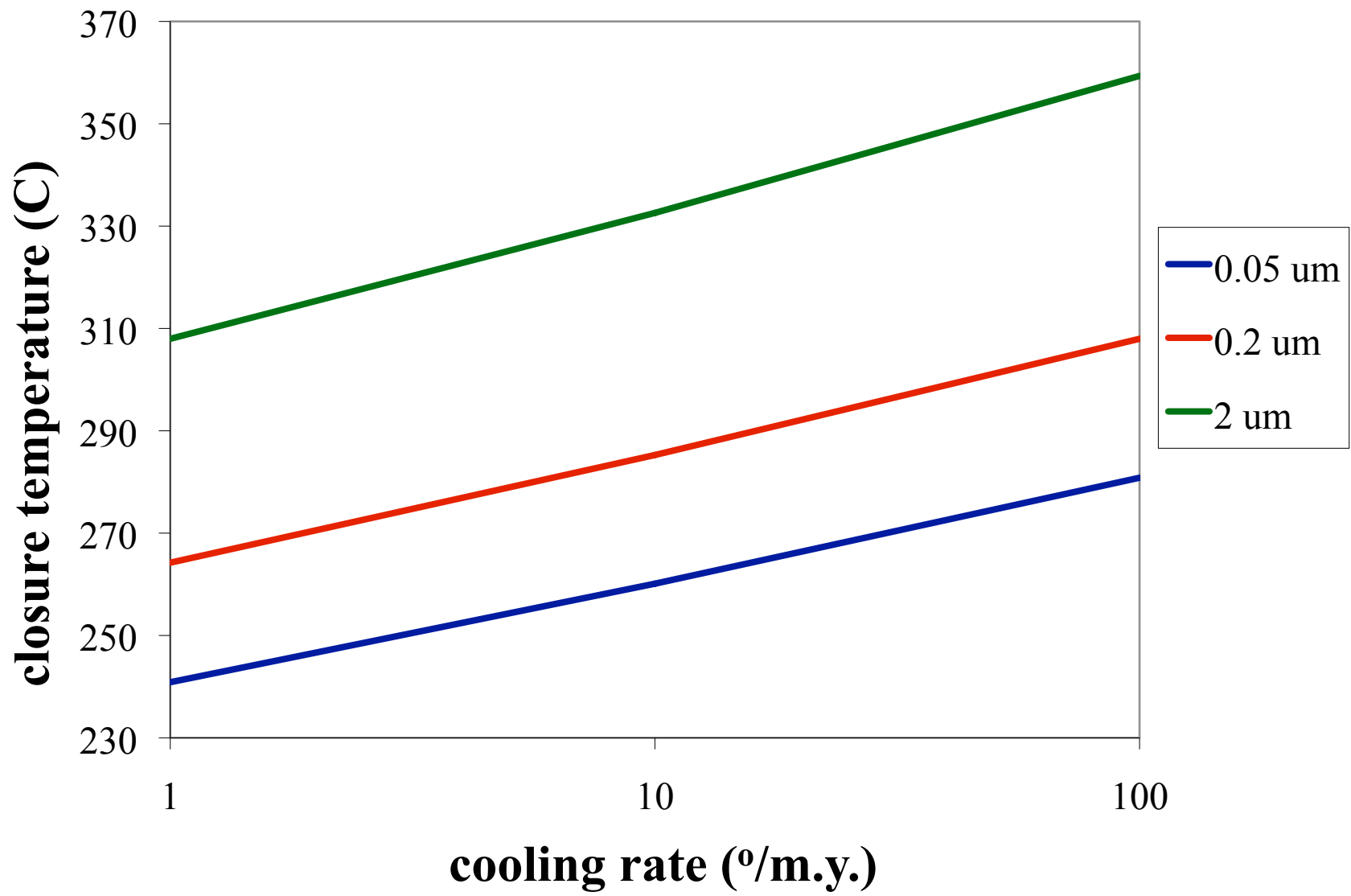


0.05 - 0.2um

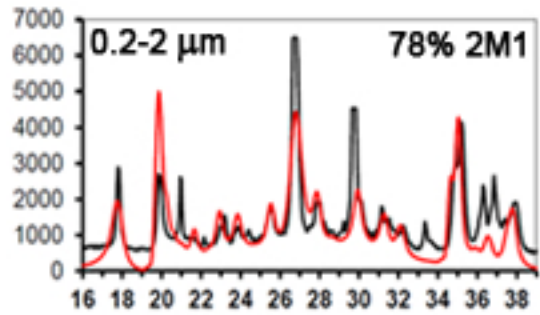


0.2 - 2um

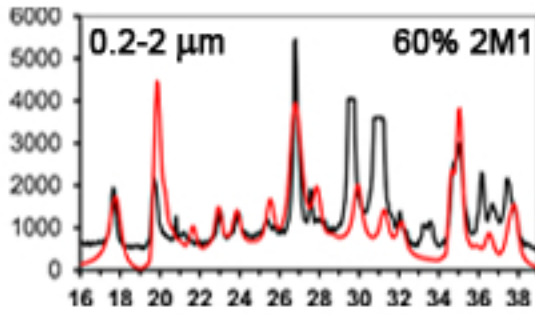




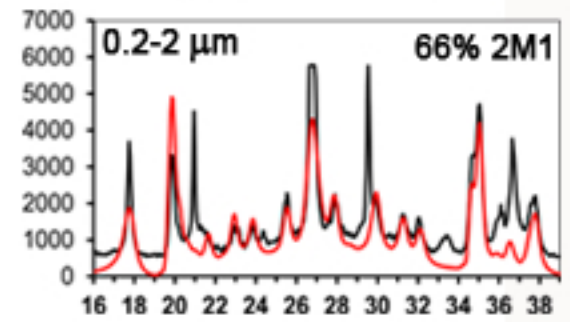
Center



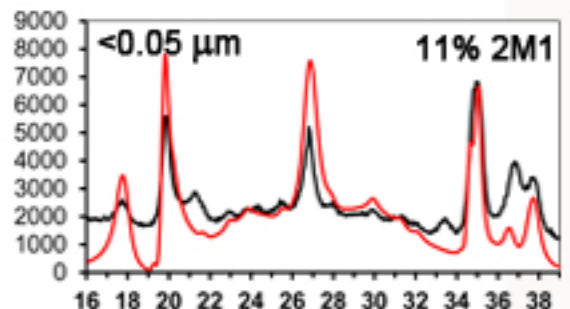
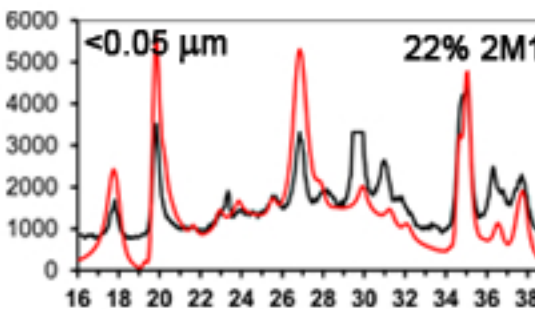
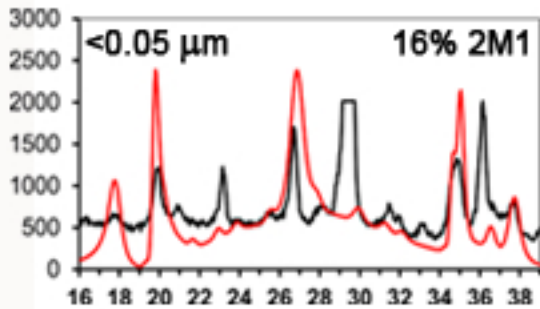
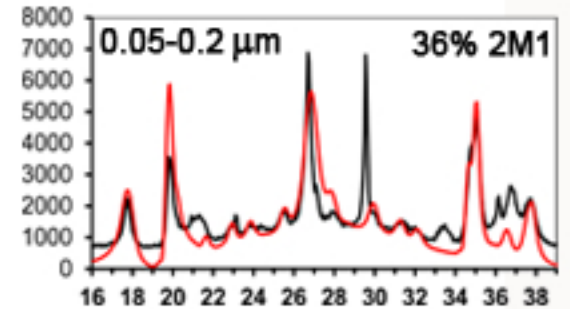
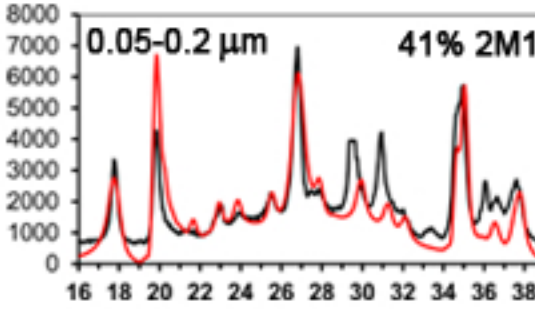
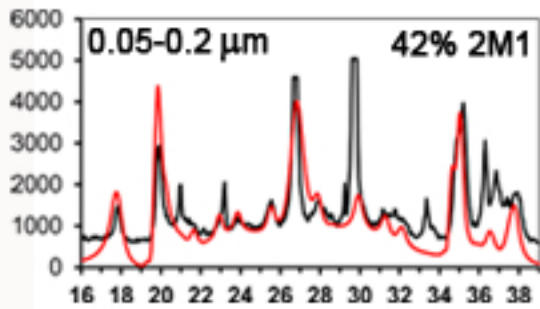
Boundary



Iberville Fm.



Intensity



3. Data Appendix

Quebec PST - Ch1

Sample #	% clast (AVG)	TGA ($\pm 2\sigma$)	exp(l.t) -1
TOQ50203(enp)			
TOQ50203-1	20	663.9 \pm 1.8	0.44484171
TOQ50203-2	13	648.2 \pm 1.7	0.43232251
TOQ50203-3	10	641.82 \pm 1.86	0.42726614
TOQ50203-4	10	641.49 \pm 1.64	0.42700509
TOQ50203-5	9	634.98 \pm 2.22	0.42186503
TOQ50203-6	9	634.7 \pm 1.63	0.42164437
TOQ50204-1	16	655.6 \pm 2.13	0.43820971
TOQ50204-2	18	659.53 \pm 2.23	0.44134611
TOQ50204-3	10	640.4 \pm 1.83	0.42614317
TOQ50204-4	13	644.45 \pm 1.89	0.42934834

Encapsulated TGA RA
 TOQ50203 610.3 \pm 4.6 619.0 \pm 2.5

Quebec fault gouge - Ch2

Fault gouge data

Sample	%2M1	weight	IC	IC_corrected		Total gas
TOQ50202_wr(F)	18			0.068	might be 50502_wr	
TOQ50202_wr(M)	37			0.068		
TOQ50202_wr(C)	55			0.068		
TOQ50204(F)	21	8.7	1.065	1.555	Montmorency falls	
TOQ50204(M)	20	8.4	1.696	2.436		
TOQ50204(C)	31			0.068		
TOQ50204_g(F)	12		1.065	1.555	Montmorency falls	
TOQ50204_g(M)	15		1.74	2.497		
TOQ50204_g(C)	25			0.068		
TOQ50406(F)_2	18		0.768	1.140	Bout de lile fault	
TOQ50406(M)_2	15			0.068		
TOQ50406(C)_2				0.068		
TOQ50406(F)	11		0.749	1.114	Bout de lile fault	382.6±0.9
TOQ50406(M)	14		0.768	1.140		406.5±1.2
TOQ50406(C)	25		0.447	0.692		478.3±1.0
TOQ50502(F)	3			0.068	Minor fault	
TOQ50502(M)	12			0.068		
TOQ50502(C)	26			0.068		
TOQ50503(F)	17			0.068		
TOQ50503(M)	19			0.068		
TOQ50503(C)	21			0.068		
TOQ50505_g(F)	redo			0.068	Faille de Ills fault	
TOQ50505_g(M)	12			0.068		
TOQ50505_g(C)	18		0.078	0.177		
TOQ50505(F)	12			0.068	Faille de Ills fault_wr	
TOQ50505(M)	15			0.068		
TOQ50505(C)	27		0.78	1.157		
TOQ50508(F)				0.068		
TOQ50508(M)	12			0.068		
TOQ50508(C)	25			0.068		
TOQ50608!(F)	2					
TOQ50608!(M)	9					
TOQ50608!(C)	35					
TOQ50701(F)	7			0.068		
TOQ50701(M)	10			0.068		
TOQ50701(C)	23		0.504	1.033		
TOQ50701!(F)	7			-0.053	Minor fault	
TOQ50701!(M)	13			-0.053		
TOQ50701!(C)	27		0.478	0.977		
TOQ50710_g(F)	9			-0.053		
TOQ50710_g(M)	16			-0.053		
TOQ50710_g(C)	32		#REF!	#REF!		
TOQ50713_core(F)				0.068	Normal fault	
TOQ50713_core(M)	18			0.068		
TOQ50713_core(C)			0.219	0.374		

Quebec fault gouge - Ch2

TOQ50713_DZ(F)	10?			0.068	Normal fault	
TOQ50713_DZ(M)			0.219	0.374		
TOQ50713_DZ(C)			0.179	0.318		
TOQ50811_core(F)	19			-0.053	Richardson thrust	342.19±0.98
TOQ50811_core(M)	36			-0.053		395.12±1.03
TOQ50811_core(C)	71		0.178	0.330		428.79±0.94
TOQ50811_DZ(F)	14			0.068		
TOQ50811_DZ(M)	27			0.068		
TOQ50811_DZ(C)	95			0.068		
TOQ51002_F(F)	7			0.068		
TOQ51002_F(M)	12			0.068		
TOQ51002_F(C)	31			0.068		
TOQ51104_core(F)	N/A	8.2	0.169	0.304	Highland Thrust_VT	
TOQ51104_core(M)	N/A	8.3	0.258	0.428		
TOQ51104_core(C)	19	9.3	0.169	0.304		
TOQ51104_DZ(F)	N/A			0.068	Highland Thrust_VT	
TOQ51104_DZ(M)	N/A			0.068		
TOQ51104_DZ(C)	26			0.068		
TOQ51203_g(F)	redo			0.068	Quarry Thrust_VT	
TOQ51203_g(M)	22		0.652	0.978		
TOQ51203_g(C)	39			0.068		
TOQ51204(F)	34	8.4		0.068	Champlain Thrust	
TOQ51204(M)	44	8.3		0.068		
TOQ51204(C)	62			0.068		
TOQ51204_margin(F)	21		0.391	0.614	Champlain Thrust	188.6±0.5
TOQ51204_margin(M)	44		0.316	0.509		212.9±0.5
TOQ51204_margin(C)	58		0.216	0.370		219.0±0.6
TOQ51204_UC(F)	13		0.515	0.787	Champlain Thrust	
TOQ51204_UC(M)	29			0.068		
TOQ51204_UC(C)	62		0.356	0.565		
TOQ51204_center(F)	16		0.255	0.424	Champlain Thrust	227.4±1.3
TOQ51204_center(M)	42		0.316	0.509		253.1±0.9
TOQ51204_center(C)	78		0.203333	0.352		326.8±0.9
	0.203	0.207	0.2	0.347		
			0.159	0.290		
			0.172	0.308		
TOV52501(F)	11			0.068	Champlain footwall	281.92±1.01
TOV52501(M)	36			0.068		295.48±1.5
TOV52501(C)	66		0.188333	0.331		324.91±1.15

Quebec fault gouge - Ch2

retention	UTM	
	Easting	Northing
	3522625	6033618
	3522685	6033642
	3455243	5859008
	3454504	5859594
522.4±1.2	3464279	5854013
542.5±1.5		
591.6±1.3	3468810	5852788
	3468706	5852793
	3495941	5846253
	3499961	5844444
	3474690	5684976
	3479196	5727404
	3478467	5733414
	3536167	5567215
	3536103	5576708
	3539169	6000392

Quebec fault gouge - Ch2

3540305 5997883

517.38±1.39 3543094 6001340

486.36±1.28

469.51±1.03

3556595 6003616

3556121 6028948

3536082 5576750

3490219 5671105

3539872 6027054

3539633 5998093

259.8±0.6 3539633 5998093

267.1±0.7

261.4±0.7

3539633 5998093

336.8±1.5 3539633 5998093

338.6±1.2

376.4±1.0

428.15±1.5

410.18±2.05

386.45±1.33

Quebec shales and slates - Ch2

Sample	%2M1	IC		UTM	
St. Lawrence transect			new	Easting	Northing
TOQ50201(F)				3500269	6018776
TOQ50201(M)	4				
TOQ50201(C)		0.896	0.968		
TOQ50202(F)				3500097	6018901
TOQ50202(M)	12				
TOQ50202(C)	18	2.002	1.921		
TOQ50102(F)				3515524	6056762
TOQ50102(M)					
TOQ50102(C)			0.196		
TOQ50101(F)				3510339	6049827
TOQ50101(M)	7				
TOQ50101(C)	12	0.7825	0.870		
TOQ50402(F)				3497486	6014954
TOQ50402(M)	11				
TOQ50402(C)	15	0.692333	0.792		
TOQ50406(F)				3499255	6016224
TOQ50406(F)	14				
TOQ50406(F)	25	#DIV/0!	#DIV/0!		
TOQ50407!(F)	9			3499915	6018780
TOQ50407!(M)	13				
TOQ50407!(C)		#DIV/0!	#DIV/0!		
TOQ50501(F)				3499903	6018774
TOQ50501(M)	4				
TOQ50501(C)	27	0.427	0.564		
TOQ50401(F)	2			3499876	6018756
TOQ50401(M)	8				
TOQ50401(C)	35	0.427667	0.564		
TOQ50503(F)	17			3499810	6018736
TOQ50503(M)	19				
TOQ50503(C)	22	0.569	0.686		
TOQ50504(F)				3500795	6008312
TOQ50504(M)	9				
TOQ50504(C)	15	0.587	0.701		
TOQ50506(F)				3500601	6008564
TOQ50506(M)	5				
TOQ50506(C)	15		0.196		
TOQ50507(F)				3503900	6014840
TOQ50507(M)					
TOQ50507(C)		0.718	0.814		
TOQ50508(F)				3502801	6015156
TOQ50508(M)	12				
TOQ50508(C)	25	0.635333	0.743		
TOQ50509(F)				3502835	6015072
TOQ50509(M)	10				

Quebec shales and slates - Ch2

TOQ50509(C)		0.6335	0.742		
TOQ50510(F)				3502857	6015010
TOQ50510(M)					
TOQ50510(C)	9	0.7	0.799		
TOQ50511(F)				3502915	6014973
TOQ50511(M)	16				
TOQ50511(C)	17	0.610333	0.722		
TOQ50601(F)				3502994	6014909
TOQ50601(M)	10				
TOQ50601(C)	18	0.7535	0.845		
TOQ50602(F)				3502994	6014908
TOQ50602(M)	8				
TOQ50602(C)	21	0.476333	0.606		
TOQ50603(F)				3502998	6014894
TOQ50603(M)					
TOQ50603(C)		0.505	0.631		
TOQ50604(F)				3503006	6014824
TOQ50604(M)	12				
TOQ50604(C)	21	0.580333	0.696		
TOQ50605(F)				3503004	6014822
TOQ50605(M)	15				
TOQ50605(C)	37	0.485333	0.614		
TOQ50606(F)				3503075	6014788
TOQ50606(M)	12				
TOQ50606(C)	36	0.7575	0.848		
TOQ50607(F)				3503208	6014772
TOQ50607(M)					
TOQ50607(C)		0.608	0.720		
TOQ50608(F)				3503587	6014701
TOQ50608(M)	9				
TOQ50608(C)	35	0.49	0.618		
TOQ50909(F)				3504090	6014975
TOQ50909(M)	12				
TOQ50909(C)	35	0.371	0.515		
TOQ50908(F)				3504130	6015033
TOQ50908(M)	12				
TOQ50908(C)	25	0.607	0.719		
TOQ50907(F)				3504213	6015336
TOQ50907(M)					
TOQ50907(C)	redo		0.196		
TOQ50906(F)				3504216	6015418
TOQ50906(M)					
TOQ50906(C)	66	0.305	0.458		
TOQ50905(F)				3504661	6015914
TOQ50905(M)	34				
TOQ50905(C)	72	0.214	0.380		
TOQ50904(F)				3504801	6015971

Quebec shales and slates - Ch2

TOQ50904(M)	35		
TOQ50904(C)	77	0.315	0.467

Chaudiere transect

TOQ50704(F)	6			3512050	6021899
TOQ50704(M)	14				
TOQ50704(C)	25	0.585	0.700		
TOQ50703(F)	8			3512353	6022262
TOQ50703(M)	11				
TOQ50703(C)	18	0.6955	0.795		
TOQ50705(F)	0			3513110	6026342
TOQ50705(M)	2				
TOQ50705(C)	5	0.46	0.592		
TOQ50706(F)	5			3513563	6028090
TOQ50706(M)	more sample				
TOQ50706(C)	58	0.379	0.522		
TOQ50716(F)	6			3516246	6032225
TOQ50716(M)	10				
TOQ50716(C)	19	0.683667	0.785		
TOQ50715(F)	9			3516307	6032755
TOQ50715(M)	18				
TOQ50715(C)	32	0.285	0.441		
TOQ50707(F)	11			3516706	6036895
TOQ50707(M)	9				
TOQ50707(C)	28	0.404	0.544		
TOQ50708(F)	9			3502387	6008397
TOQ50708(M)					
TOQ50708(C)	34	0.481333	0.610		
TOQ50709(F)	9			3502020	5998661
TOQ50709(M)	12				
TOQ50709(C)	36	0.26	0.420		
TOQ50710(F)	9			3499200	5996550
TOQ50710(M)	16				
TOQ50710(C)	32	0.308	0.461		
TOQ50714(F)	12			3506815	5993623
TOQ50714(M)	18				
TOQ50714(C)	45	0.251667	0.413		
TOQ50713(F)	22			3508321	5988957
TOQ50713(M)	38				
TOQ50713(C)	81	0.196	0.365		
TOQ50711(F)	N/A			3513183	5984426
TOQ50711(M)	36				
TOQ50711(C)	84	0.109333	0.290		
TOQ50712(F)	N/A			3516926	5981779
TOQ50712(M)	32				
TOQ50712(C)	92	0.108667	0.289		

Quebec shales and slates - Ch2

Etchemin transect

TOQ50302(F)	N/A			3524767	5981583
TOQ50302(M)	7				
TOQ50302(C)	11	0.506	0.632		
TOQ50701(F)	7			3525811	5981998
TOQ50701(M)	10				
TOQ50701(C)	23	0.504	0.630		
TOQ50801(F)	14			3542129	5975539
TOQ50801(M)	16				
TOQ50801(C)	18	0.433667	0.569		
TOQ50803(F)	14			3542876	5975401
TOQ50803(M)	18				
TOQ50803(C)	27	0.395333	0.536		
TOQ50805(F)	12			3534965	5980166
TOQ50805(M)	21				
TOQ50805(C)	44	0.190333	0.360		
TOQ50804(F)	4			3534988	5980152
TOQ50804(M)	16				
TOQ50804(C)	29	0.517	0.641		
TOQ50806(F)	7			3531748	5982284
TOQ50806(M)	12				
TOQ50806(C)	31	0.248333	0.410		
TOQ50807(F)	13			3512465	5987154
TOQ50807(M)	19				
TOQ50807(C)	35	0.273333	0.431		
TOQ50808(F)				3508630	5989648
TOQ50808(M)					
TOQ50808(C)		0.283667	0.440		
TOQ50811(F)				3510945	6003370
TOQ50811(M)	36				
TOQ50811(C)	71	0.170667	0.343		
TOQ50810(F)				3512363	6002654
TOQ50810(M)	18				
TOQ50810(C)	44	0.28	0.437		
TOQ50809(F)				3520032	5998008
TOQ50809(M)	43				
TOQ50809(C)	77	0.2645	0.424		
TOQ50812(F)				3524407	5997025
TOQ50812(M)	22				
TOQ50812(C)		0.259	0.419		
TOQ50813(F)	28			3524000	5996826
TOQ50813(M)	42				
TOQ50813(C)	100	0.138333	0.315		
TOQ50814(F)				3528342	5997734
TOQ50814(M)	57				
TOQ50814(C)	82	0.225	0.390		
TOQ50815(F)				3528594	5998628

Quebec shales and slates - Ch2

TOQ50815(M)	45				
TOQ50815(C)		0.147	0.322		
TOQ50902(F)				3532522	5999249
TOQ50902(M)	N/A				
TOQ50902(C)	62	0.144	0.320		
TOQ50903(F)				3539317	5999820
TOQ50903(M)					
TOQ50903(C)			0.196		
TOQ50901(F)				3539075	6001321
TOQ50901(M)	redo				
TOQ50901(C)	88		0.196		
TOQ51010(F)				3539044	6000377
TOQ51010(M)	11				
TOQ51010(C)	17	1.091667	1.136		
TOQ51101(F)				3539098	6000376
TOQ51101(M)	9				
TOQ51101(C)	16	0.953333	1.017		
TOQ50911(F)				3539169	6000392
TOQ50911(M)					
TOQ50911(C)	23	0.545	0.665		
TOQ50910(F)				3539633	5998093
TOQ50910(M)	16				
TOQ50910(C)	24	0.245	0.407		
TOQ51001(F)				3540305	5997883
TOQ51001(M)	N/A				
TOQ51001(C)	32		0.196		
TOQ51002(F)	8			3540634	5997805
TOQ51002(M)	16				
TOQ51002(C)	34	0.432333	0.568		
TOQ51009(F)				3543094	6001340
TOQ51009(M)	15				
TOQ51009(C)	41	0.248333	0.410		
TOQ51008(F)	15			3557149	5996744
TOQ51008(M)	35				
TOQ51008(C)	59	0.128	0.306		
TOQ51007(F)				3556595	6003616
TOQ51007(M)	52				
TOQ51007(C)	100	0.154	0.328		
TOQ51003(F)				3557094	6005707
TOQ51003(M)	35				
TOQ51003(C)	85	0.186	0.356		
TOQ51004(F)				3556121	6028948
TOQ51004(M)	N/A				
TOQ51004(C)	62	0.155333	0.330		
TOQ51005(F)				3544670	6027163

Quebec shales and slates - Ch2

TOQ51005(M)	37			
TOQ51005(C)	88	0.168667	0.341	
TOQ51006(F)				3539872 6027054
TOQ51006(M)	41			
TOQ51006(C)	100	0.11	0.290	